ABSTRACT

Title of Thesis: A POTENTIAL FLOW MODEL OF A FIRE SPRINKLER HEAD

Taylor Myers, Master of Science, 2014

Dissertation directed by: Professor André Marshall
Department of Fire Protection Engineering

Understanding fire sprinkler sprays fills a critical gap in the modeling of fire suppression systems. Previous research has shown that a modeling framework consisting of an instability model coupled with a stochastic transport model can paint most of the sprinkler spray picture, but requires input in the form of the thickness and velocity of unstable fluid sheets. The model outlined forgoes traditional CFD to solve for water jet-deflector interactions, and instead describes the sheet formation as a potential flow boundary value problem, utilizing a free surface formulation and the superposition of the Green's function. The resulting model allows for the determination of the complete flow field over a fire sprinkler head of arbitrary geometry and input conditions. A hypothetical axisymmetric sprinkler is explored to provide insight into the impact of sprinkler head geometry on local fluid as well as complete spray behavior. The resulting flow splits, sheet thicknesses, and sheet velocities are presented for various sprinkler head geometries.

A POTENTIAL FLOW MODEL OF A FIRE SPRINKLER HEAD

by

Taylor Myers

Thesis submitted to the Faculty of the Graduate School of the
University of Maryland, College Park in partial fulfillment
of the requirements for the degree of
Master of Science
2014

Advisory Committee:
Professor André W. Marshall, Chair
Professor Howard Baum
Professor Arnaud Trouvé
Professor Michael Gollner

Table of Contents

List of Figures

Nomenclature

A_s	area of deflector plate openings
f	free-surface location
G	Green's function
G_1	Green's function with a plate at $z = 0$
$\mathcal{G}$	axisymmetric Green's function
$\mathcal{G}_\infty$	axisymmetric Green's function with a plate at $z = 0$
J_0	Bessel function of order zero
p	pressure of fluid
p_s	static pressure of fluid
R_j	radius of jet boundary
R_s	radius of the centroid of the slot
R_D	radius of the deflector plate
R_{ts}	arbitrary radius of tine stream boundary
ΔR	width of the slot
$\vec{r}$	spatial location
$\vec{r}_0$	source location
r	radius
r_0	source radius
T_s	slot sheet thickness
T_T	tine sheet thickness
U_j	jet velocity
u	radial velocity
v	vertical velocity
Z_j	arbitrary height of jet boundary
z	height
z_0	source height
z_s	tine sheet thickness

Greek

α	flow split
δ	Dirac Delta function
λ_n	Eigenvalue of the order zero Bessel function
θ	angular spatial location
θ_s	trajectory angle of slot sheets
θ_t	trajectory angle of tine sheets
ρ	fluid density
Φ	perturbation potential
ϕ	fluid potential

Chapter 1: Introduction

1.1 Motivation

Sprinkler systems are a ubiquitous form of fire protection in the United States with expanding adoption around the world. The performance of a sprinkler depends on the spray generated by the sprinkler, the dispersion of the spray within the flames, and the wetting of burning surfaces. Despite the widespread use of sprinklers, analytical models to predict their performance have yet to be developed. Each one of these stages of sprinkler modeling involve complex transport processes which create important modeling and measurement challenges. The transport processes responsible for sprinkler performance are complex, not readily yielding to measurement or analysis, making the development of analytical models difficult.

The possibility of accurately predicting water delivery with fire models, or more ambitiously, of designing sprinklers with models to produce particular sprays, has far reaching implications for suppression technology and engineering practices. Previous research by Ren [1] has outlined a three part modeling framework by which a typical sprinkler's atomization mechanism can be predicted. Figure 1.1 shows the three steps to predicting a sprinkler spray. First, a fluid jet impinges upon a deflector of some geometry and is transformed into an array of fluid sheets which

carry the flow of the sprinkler away from the deflector. Second, these sheets undergo aerodynamic instabilities and break apart, first into ligaments and then droplets. Third, the transport of these sheet fragments away from the deflector and outwards into the environment are characterized.

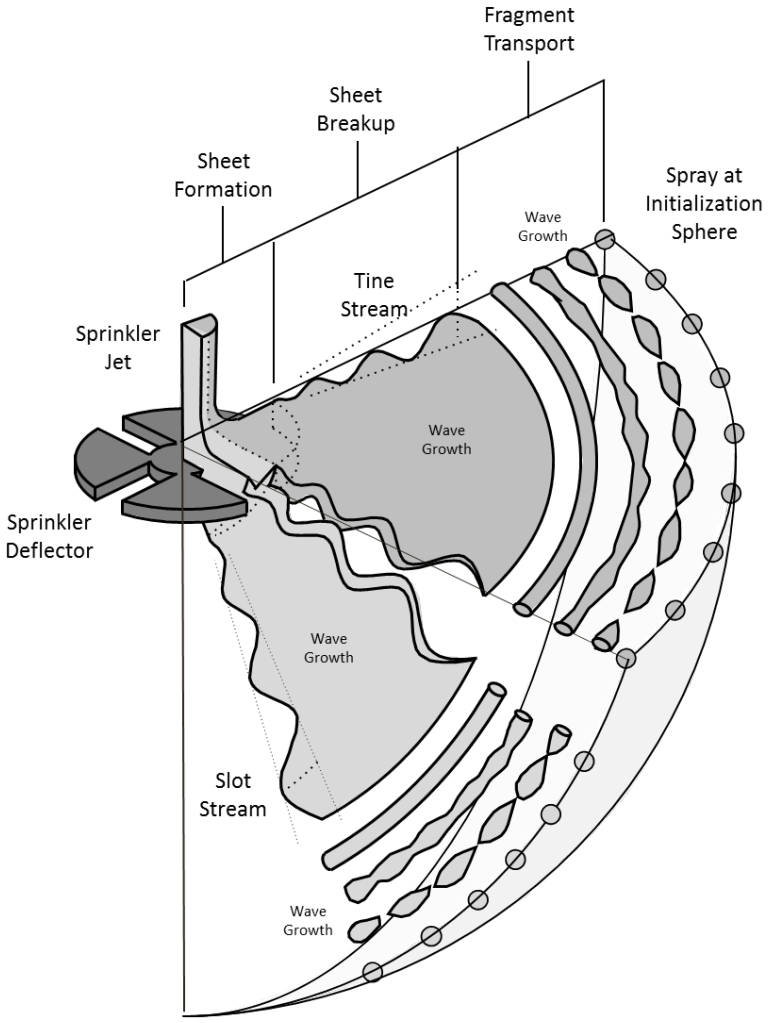

Figure 1.1: An illustration of a three part model for sprinkler patternation and droplet formation.

The first model, the sheet formation model, is particularly important to determining overall sprinkler performance. Research by Ren [2] developed scaling laws governing drop formation based upon initial sheet properties. These sheet proper-

ties are an output of the sheet formation model. Additional research by the author has suggested that patternation and spread of the fragments, the primary goal of the fragment transport model, are determined by patternation and thickness of the initial sheets, also outputs of the sheet formation model. The sheet formation model is then critically important to understanding total sprinkler behavior.

The goal of a sheet formation model is to take the initial conditions of a sprinkler (the total flow, pressure, and geometry) and to produce the initial conditions for a sheet breakup model (sheet location, velocity, and thickness). With the appropriate nondimensionalization, explored in Sec. 2.3, the model can be reduced to solving for the sheet location, sheet trajectory angle, and sheet thickness.

The goal of the present research is to introduce a general scheme for predicting sheet formation from the impingement of a jet onto a deflector and to provide insight into how deflectors govern sprinkler spray behavior and represent an important fundamental sub-model required for predicting the initial sprinkler spray. In previous efforts by the author, a traditional computational fluid dynamics (CFD) approach have been used in an attempt to characterize the sheet formation model. In a traditional CFD approach tremendously detailed griding is required to resolve the thin sheets (on the order of 50 microns). As a result, the computational expense necessary to explore even a single sprinkler geometry is large. If an understanding of the impacts of plate geometry on sheet formation are to be understood, a large number of computations must be run.

A new and more efficient alternative formulation for the sprinkler head deflector flow problem is posed based on free streamline flow theory. A free surface

describes the surface of a fluid that is subject to constant perpendicular normal stress. The boundary between two homogeneous fluids; in this case, the impinging water jet and the surrounding air, can be described as a constant pressure free surface. Because of this constant pressure free surface description of the jet, it is known that there is no flow normal to the jet boundary and thus the liquid-air boundary is a free streamline. The essential notion is to make use of the fact that a free surface model of the flow can be constructed, where all of the vorticity of the flow is contained within the free surface, and the interior of the water jet as a velocity potential. Using the potential flow assumptions, the fluid velocity potential solutions can be reduced to a boundary value problem. Any solution obtained is an exact solution of the inviscid potential flow equations, and the interior flow is an exact solution of the Navier-Stokes equations. The resulting model is as accurate as a CFD approach assuming the same assumptions and calculation precision.

One of the primary assumptions of the above model are that the inviscid potential flow assumptions are valid for the domain of jet impinging on a sprinkler head. In reality almost any fluid problem is non-conservative, but the impacts of viscosity, surface tension, and turbulence are minor on the scales associated with a sprinkler head. For the speed and length scales associated with sprinklers (on the order of 0.01 m and 10 m/s, or a Reynolds number of 10^5) a viscous boundary layer thickness of less than 5% of the total sheet thickness is expected, allowing viscous effects to be neglected in the primary portion of the flow [3]. Viscous effects of slot flow can be accounted for with a slot flow coefficient as outlined in Section 2.4. All of the vorticity in the flow is captured in the free surface, a vortex sheet, with the

internal flow remaining irrotational.

This is not to suggest that the impacts of viscosity, turbulence, and surface tension are negligible for the sprinkler problem. Viscosity, surface tension, and turbulent perturbations all play a large role in the sheet break up sub-model of the sprinkler modeling framework, as discussed in work by Ren [2]. These effects are unimportant, however, for the sheet formation model.

Simplifying the sprinkler sheet formation model to a boundary value problem dramatically reduces the computational expense. This is the result of minimizing the number of computations which must be run in order to determine a value of interest within the domain. In traditional CFD, a solution is reached by solving for the total flow at every point within a domain. For flows with small regions of interest, like the thin fluid gas interface on a sprinkler head flow, this is a tremendously large number of points. Additionally, these CFD formulations are unsteady, and in order to assure instabilities do not affect the problem, even smaller time steps must be chosen. In a boundary value problem formation, like the formulation to be used here, any point in the domain can be solved for using only the values at the boundaries, as shown in Fig. 1.2. The result is the ability to recover important sheet formation outputs: like flow split (the fraction of the total flow which passes through the deflector, as shown in Fig. 1.1) or sheet thickness.

By reducing the computational load, the parameter space for sprinkler head geometry can be more thoroughly explored, and the impact of geometric parameters on the sheet formation and ultimately the sprinkler spray can be more completely understood.

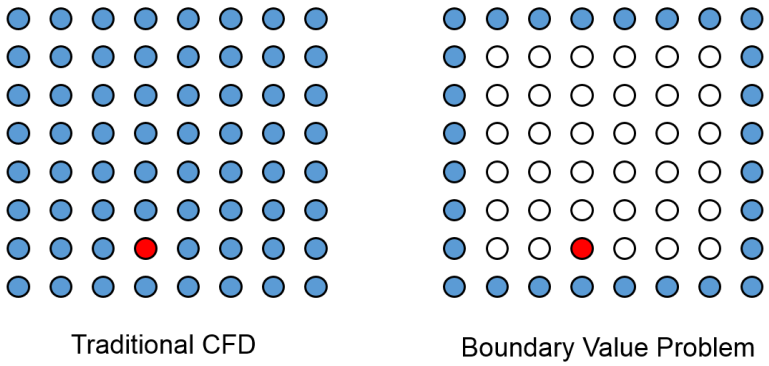

Figure 1.2: An illustration of the points and thus calculations required (blue points) to recover a particular quanitity of interest (red points) for traditional CFD and the boundary value approach outlined in this thesis.

1.2 Literature Review

A wealth of literature exists studying sprays of all formulations. Fire sprinklers however are a fairly uncharacterized technology. The work outlined by the author relies on an understanding of an only loosely connected body of work. First, an important aspect is the general atomization mechanisms of sprays. Atomization in sprinkler sprays in particular are not well explored, but a history of studying sprays in general dates back centuries. An understanding of the parameters which control atomization is necessary to inform the design of a model which will in turn provide these parameters to determine spray characteristics. Second, previous deflector models. Some limited work has been performed modeling deflectors in the past. Though none of these models use the same methodology for predicting deflector interactions they do provide insight into the process. Lastly, an understanding of potential flow formulations, their applications, and limitations is critical to the formation of this particular model. The model outlined in this thesis relies upon

potential flow theory. Previous work utilizing potential flows to predict a variety of fluid conditions informs the deflector model.

1.2.1 Atomization Mechanisms

The description of a liquid sheet is of critical importance to the determination of sprinkler sprays because the properties of said sheet govern atomization and droplet spread. When a narrow liquid stream is injected into a gaseous fluid, it tends to break up into fragments due to surface tension and/or aerodynamic forces. Atomization of liquid sheets was first studied by Savart [4] in 1833 who observed break-up phenomena of radial expanding sheets produced by two co-axial colliding jets. It was observed that when thin liquid sheets are generated in the atmosphere, unstable sinuous waves are formed. Jet atomization was first studied by Rayleigh [5], who found that if the ambient gas and liquid viscosity were neglected, the jet is most susceptible to disturbances having wavelengths 1.43 times the jet circumference. A more sophisticated model was developed by Weber [6] in 1931, including the effect of liquid viscosity and density of the ambient gas.

Squire [7] first solved the linearized equation for parallel liquid sheet instability. Hagerty and Shea [8] found that under normal operating conditions, the wavelength is relatively large compared to the sheet thickness and their growth rates are consequently greater than those of the alternative dilatational forms typical of the jet atomization studied by Rayleigh. Dombrowski [9–11] studied the effect of ambient density on drop formation in sheet based fan-spray nozzle experiments. Dombrowski

determined the fastest growing wave (most unstable) that caused the sheet to break up. For inviscid sheets, he determined the critical wavelength, $\lambda_{crit} = 4\pi\sigma\rho_a U^2$, where σ is the surface tension of liquid, ρ_a is the density of ambient gas, and U is the characteristic velocity of the sheets. He also suggested an approach for determining the critical wavelength for viscous sheets. Li and Tankin [12], Huang [13], and Clanet and Villermaux [14, 15] all studied the break-up of liquid sheets generated by liquid jets impinging onto a small deflector.

Further research by Ren [1] studied the applicability of Dombrowski's droplet break up scheme to sprays generated by fire sprinkler nozzles. Ren divided the process into a series of instability developments and growths. Fig. 1.1 shows this proposed process. First sheets leaving the fire sprinkler deflector form. These sheets develop instabilities and break apart, in a manner dictated by Dombrowski's inviscid wave growth equations, into ligaments. These ligaments in turn develop instabilities by the Rayleigh instability mechanism and break apart into droplets. Through this analysis Ren was able to develop scaling laws governing drop formation based upon initial sheet properties. These scaling laws allow the determination of drop size based upon initial sheet thickness.

1.2.2 Deflector Models

A few attempts have been made previously to attempt to model behavior on a fire sprinkler head. Owing to the complex nature of sprinkler heads, and thus the necessarily chaotic behavior flow impinging on these heads, dramatic simplifications

have been necessary.

Schach [16] characterized the deflection of an axisymmetric water jet on a flat plate perpendicular and oblique to the flow direction using the Prandtl hodograph method. The free surface of the the outer jet was compared with previous experimental measurements [17] represented by an empirical equation. The problem is also discussed mathematically. In the paper a method for treating the flow using potential flow assumptions is outlined. The method calls for the transformation of a differential equation of the fluid potential into an integral equation for axisymetric flow by superposition of a ring flow. Schach identifies the chief problem with the formulated solution is the lack of a known shape for the free surface boundary (in the paper referred to as the "jet edge"). For a true potential flow where all flow is deflected by the plate, the flow approaches a hyperbola as approaches an infinite radius. Further along the free surface the fluid has a constant speed equal to the inlet speed.

Prahl [18], in 1988, attempted to calculate the discharge distribution for an axisymmetric model of a fire sprinkler head. A non-dimensional description was used which emphasized a sprinklers ability to evenly distribute spray over a maximum possible floor area. The axisymmetric sprinkler used consisted of a jet impinging normal to and at the center of a flat disk. From there mass conservation assumptions were utilized to approximate sheet thickness and velocity and the previously mentioned Dombrowski model for sheet break up was used to understand droplet formation. The model presented lends insight into the parameters of a sprinkler spray but is overly simplistic, allowing for no flow to pass through the deflector

plate as is characteristic of the canonical configuration.

Ren, in later unpublished work explored the usage of computational fluid dynamics (CFD) in the modeling of traditional pendant sprinkler heads. In a preliminary study to address the challenge of locating the liquid-gas interface (and the associated sheet thickness and velocity), the Volume of Fluid (VOF) method as outlined in Hirt [19] was applied to a sprinkler-head simulation. The VOF method is a simple but powerful approach designed with the goal of tracking the shape and position of the interface during multi-phase CFD simulations. However, the computational burden to calculate the gas flow, liquid flow, and their interactions during the CFD based sprinkler-head simulation was prohibitive owing to mesh requirements for resolution of the thin sheets (with typical grid sizes of tens of microns) formed by the deflector (with typical sizes of tens of millimeters).

1.2.3 Potential Flow Formulations

There is a tremendous amount of literature describing the usage of potential flow in solving two-dimensional free streamline flows dating back to the late nineteenth century. Potential flow describes a velocity field as the gradient of the scalar velocity potential function. A potential flow is characterized by an irrotational velocity field, a valid approximation for a number of cases. Two dimensional problems have typically been addressed using the hodograph method, which uses the velocity components as independent variables. Several of these classical solutions are described by Batchelor [3].

These flows are typically characterized by the the fact that the solid boundaries are composed of straight line segments, while the free surface is a streamline at a constant pressure, or the arc of a circle in the hodograph plane. These qualities make to relatively easy to determine the boundary shape in the hodograph plane, and the fact that the velocity components are functions of a complex variable makes conformal mapping a powerful tool in constructing the solution.

Bloomer [20] studied the incorporation of ring singularities in an axisymmetric potential field. Bloomer found that a reasonable approximation of ring singularities in a three-dimensional potential field having axial symmetry, by consideration of the very much easier case of a similar two-dimensional potential function. It is seen that the traces of these ring singularities on a plane through the axis of symmetry occur at points corresponding to those of the singularities existing in the two-dimensional plane when the axial velocity potential functions are the same.

Chang and Conly [21] constructed a potential flow solution describing segmented jet deflectors. The solution was constructed for a series of inviscid, incompressible, two-dimensional jets by a series of straight segments of arbitrary lengths and angles. They used a Schwarz-Christoffel mapping, or a complex conformal transformation, coupled with free streamline theory. Results showed good agreement between the potential flow approximation and previous testing of several specific cases.

In fire protection, Steckler, et. al. [22] studied fire induced flow through a compartment doorway. Transformation into the hodograph plane was used to calculate flow coefficients for smoke flow leaving the room, here posed as a inviscid,

irrotational jet. Elcrat and Zanellli [23] also modeled invicid wakes past a normal plate using a potential flow formulation. Here again flow solutions were reached through transformation into the hodograph plane.

None of these formulations operate in precisely the same framework as the sprinkler head model outlined below. In three dimensions the hodograph method is no longer available, nor is the use of complex variable techniques. However, the potential flow still satisfies the Laplace equation, and the free streamline is still a constant pressure surface, allowing many of the approximations to still hold.

1.2.4 Research Objectives

The goal of the present research is to outline a new general formulation by which sheet formation on a sprinkler head can be predicted. Further, this research seeks to understand the fundamental impact of sprinkler head geometry on fundamental parameters of a fire sprinkler, namely flow split, fluid sheet thickness, and sheet velocity. This formulation will be demonstrated through the example of an axisymmetric sprinkler with a ring slot penetration. The modeling approach for the potential flow formulation follows.

Chapter 2: Modeling Approach

2.1 Potential Flow Formulation

In three dimensions the hodograph method for solving potential flows is no longer available, nor is the use of complex variable techniques. However, the potential flow still satisfies the Laplace's equation and the free streamline remains a constant pressure surface. The free streamlines separating the water jet from the surrounding air are taken to be vortex sheets and the air is assumed to be at rest. The following method relies on the existence of a Green's function satisfying the potential flow equation and appropriate boundary and symmetry conditions. In mathematics, a Green's function is a specific type of function used to solve inhomogeneous differential equations. It is a function which transforms a boundary value of a function into the function's response to the boundary value across all space. Physically the Green's function may be thought of as a weighting function or a propagator function. $G(\vec{r}, \vec{r}_0)$ gives the effect of a unit point source ar $\vec{r}_0$ producing a potential at $\vec{r}$, as in Fig. 2.1.

The formulation of the boundary value problem in terms of an appropriate characteristic Green's function reduces the problem to the determination of the shape of the free surface and the outflow conditions on the deflector plate. The

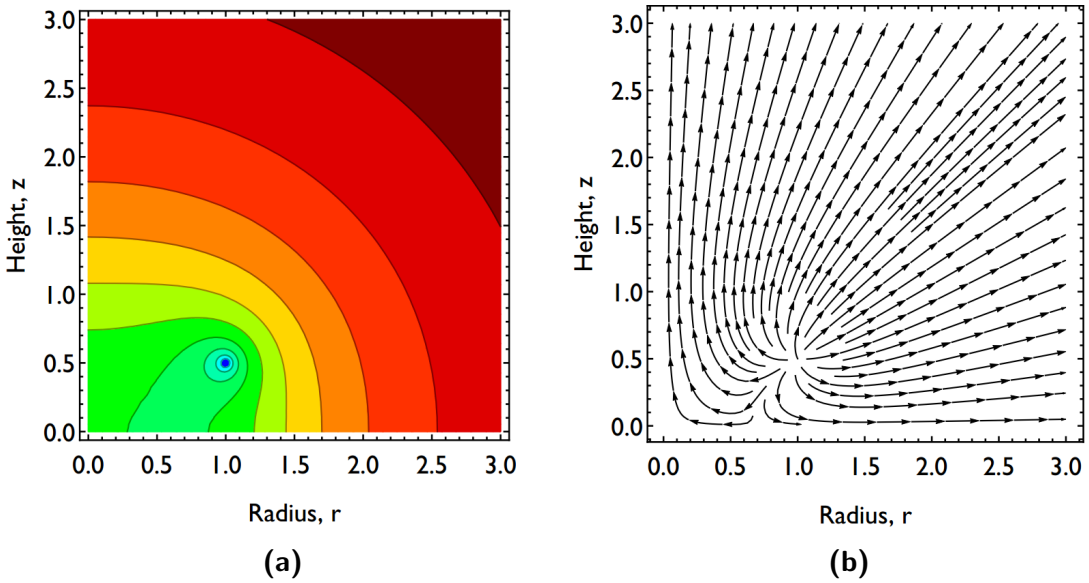

Figure 2.1: A contour plot (a) and streamlines (b) of a Green's function ($\mathcal{G}_1$), with a no flow condition across the radial axis, with a source $r_0 = 1.0$ and $z_0 = 0.5$.

boundary conditions required for definition of the Green's functions are dictated by the description of the sprinkler geometry and the nature of the incoming flow.

The general nature of the model presented in this study provides the capability of capturing the critical sheet behavior for fire sprinklers of almost any design complexity. It shares the advantage of the VOF method in being able to precisely capture interface location as well as the ability of the CFD model to exactly model the fluid flow. It achieves both of these goals with relatively minimal computational burden.

2.2 Mathematical Model

To begin development of the mathematical model, the problem is posed in cylindrical coordinates as follows. The spatial location is given as

$$\vec{r} = (x, y, z) = (r\ \cos\theta, r\ \sin\theta, z) \tag{2.1}$$

and a source location given as

$$\vec{r_0} = (x_0, y_0, z_0) = (r_0\ \cos\theta_0, r_0\ \sin\theta_0, z_0). \tag{2.2}$$

The starting point of the mathematical formulation is the assumption that, because of the size and speeds associated with sprinkler heads (a Reynold's number of $Re = 10^5$), the effects of gravity and boundary layers can be disregarded. We can then define an impinging jet velocity field, $\vec{u}(\vec{r})$, which can be described as a potential flow satisfying the equation

$$\nabla^2\phi\left(\vec{r}\right) = 0, \qquad \text{where} \qquad \vec{u}\left(\vec{r}\right) = \nabla\phi\left(\vec{r}\right). \tag{2.3}$$

The velocity, $\vec{u}\left(\vec{r}\right)$, is always perpendicular to the isocontours of $\phi\left(\vec{r}\right)$. The gauge pressure, $p_{total} - p_\infty$, is determined by the gravity free Bernoulli equation given by

$$p_{total} - p_\infty = \frac{u^2}{2} + \frac{v^2}{2} + \frac{p_s}{\rho} = constant = U_j^2/2. \tag{2.4}$$

where U_j is the velocity of the impinging jet.

Having established these preliminaries, the sprinkler boundary value problem can now be formulated. By definition, the Green's function is a solution to

$$\nabla^2 G\left(\vec{r},\, \vec{r}_0\right) = \delta\left(\vec{r} - \vec{r}_0\right). \tag{2.5}$$

Here δ denotes the Dirac Delta function in three spatial dimensions. The Dirac Delta function has the funamental property that

$$\int f(x)\delta(x-a)dx = f(a). \tag{2.6}$$

We can thus consider that $\phi(\vec{r})$ can be defined by the volume integral

$$\phi(\vec{r}) = \int \phi(\vec{r}_0)\delta\left(\vec{r} - \vec{r}_0\right) d\vec{r}_0. \tag{2.7}$$

From Eqs. 2.3, 2.5, and 2.7, $\phi(\vec{r})$ can be defined as the integral

$$\phi(\vec{r}) = \int \left[\phi(\vec{r}_0)\nabla^2 G\left(\vec{r},\, \vec{r}_0\right) - \nabla^2\phi(\vec{r}_0) G\left(\vec{r},\, \vec{r}_0\right)\right] d^3\vec{r}_0 \tag{2.8}$$

The integral above is taken over the entire volume of the flow being solved. In the general case, this volume includes the jet bounded by the inlet, its free-surface, and the deflector that it impinges on. It is important to note that this formulation by itself assumes nothing about the geometry of the problem.

Second, $\phi(\vec{r})$ can be written in the form

$$\phi\left(\vec{r}\right) = \int \nabla \cdot \left[\phi\left(\vec{r}_0\right) \nabla G\left(\vec{r},\, \vec{r}_0\right) - \nabla \phi\left(\vec{r}_0\right) G\left(\vec{r},\, \vec{r}_0\right)\right] d^3\vec{r}_0. \tag{2.9}$$

Using the divergence theorem, the above can be rewritten as

$$\phi\left(\vec{r}\right) = \oint \left[\phi\left(\vec{r}_s\right) \frac{\partial G}{\partial n}\left(\vec{r},\, \vec{r}_s\right) - G\left(\vec{r},\, \vec{r}_s\right) \frac{\partial \phi}{\partial n}\left(\vec{r}_s\right)\right] d^2s. \tag{2.10}$$

The integral in Eq. 2.10 is taken over the surface which bounds the volume of interest. Here, $\hat{n}$ is the local coordinate unit normal to the bounding surface pointing outward from the volume and $\vec{r}_s$ points along that surface.

This result is very general and assumes nothing about the specific boundary conditions or the shape of the boundaries that are needed to obtain it. To proceed further it is necessary to specify the information available to formulate a specific boundary value problem relevant to the sprinkler jet impingement on a given deflector plate. The unknowns are, as mentioned above, the values of $\phi(\vec{r})$ along the boundaries or the fluid velocity normal to the boundaries. The choice of Green's function will be considered next.

The starting point is the observation that the simplest Green's function satisfying Eq. 2.5, denoted here by $G_0\left(\vec{r},\, r_o,\, \theta_o,\, z_o\right)$, is

$$G_0\left(\vec{r},\, r_o,\, \theta_o,\, z_o\right) = -\frac{1}{4\pi}\frac{1}{|\vec{r} - \vec{r}_o|} = -\frac{1}{4\pi}\frac{1}{\sqrt{r^2 + r_o^2 - 2rr_o\cos(\theta - \theta_o) + (z - z_o)^2}}. \tag{2.11}$$

This solution satisfies Eq. 2.5, but is not particularly useful. There exist a variety of solutions to Eq. 2.5, all of which are acceptable Green's functions for use in the solution of Eq. 2.10. A simple modification can be made for the case of a planar barrier located at $z_0 = 0$, a reasonable approximation to a sprinkler deflector. The appropriate Green's function is then

$$G_1\left(\vec{r},\, r_o,\, \theta_o,\, z_o\right) = G_0\left(\vec{r},\, r_o,\, \theta_o,\, z_o\right) + G_0\left(\vec{r},\, r_o,\, \theta_o,\, -z_o\right). \tag{2.12}$$

The new solution still satisfies Eq. 2.5 and also satisfies the condition of no normal gradient at the surface $z_o = 0$. Figure 2.1 shows G_1 for a source located at $r_0 = 1$, $z_0 = 0.5$. Because the velocity component normal to the barrier either vanishes or is prescribed everywhere, the first term in Eq. 2.9 vanishes along the deflector boundary allowing the integral along the deflector boundary to be solved with only knowledge of the Green's function and the velocity normal to the deflector plate.

The Green's function can be further modified depending on the specific problem being considered. The particular choice of Green's function provides a limited amount of constraint to the problem. The remainder of the constraint will follow from the boundary conditions chosen and will reflect the geometry of the specific problem. In order to generally explore the impact of changing boundary conditions the major simplification of an axisymmetric flow pattern will be introduced in the following section.

2.3 Axisymmetric Model

The full form of the boundary value problem is quite general and can be applied to complex boundary shapes. This complexity can make explaining the modeling approach difficult and obscure the impact of essential sprinkler geometric features. In an effort to provide insight into the impact of variations of the boundary conditions, as well as to clarify the general formulation of the boundary problem, a non-dimensional axisymmetric model will be demonstrated next.

Before proceeding to explore the boundary conditions, it is useful to introduce the dimensionless variables

$$\phi = U_j R_j \tilde{\phi}(\tilde{r}, \tilde{z}), \qquad \tilde{r} = r/R_j, \qquad \tilde{z} = z/R_j, \qquad \tilde{u} = \frac{\partial \tilde{\phi}}{\partial \tilde{r}}, \qquad \tilde{v} = \frac{\partial \tilde{\phi}}{\partial \tilde{z}}. \tag{2.13}$$

The tilde notation will be dropped for the remainder of the paper for the convenience of the vector notation. Owing to this non-dimensionalization $R_j = 1$ and $U_j = 1$.

The axially symmetric form of the potential flow equation is given by

$$\frac{1}{r}\frac{\partial}{\partial r}\left(r\frac{\partial \phi}{\partial r}\right) + \frac{\partial^2 \phi}{\partial z^2} = 0. \tag{2.14}$$

The axisymmetric model suggested here is posed as follows: an inviscid, vertical jet with radius R_j impinges upon a horizontal deflector plate. A ring opening with centroid R_s and total area A_s is located in the deflector plate. Here both slot centroid, R_s, and slot area, A_s, are non-dimensionalized by the impinging jet radius and area, R_j and πR_j^2, respectively. The nondimensional slot width, ΔR, can than

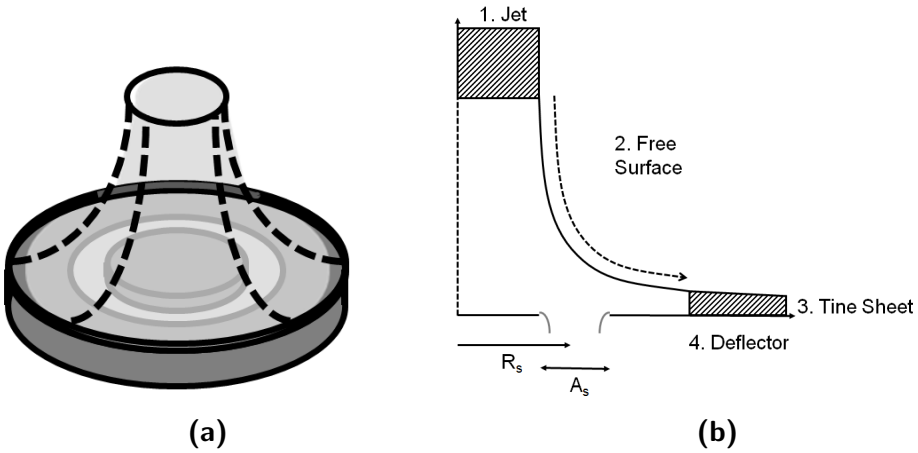

Figure 2.2: An axisymmetric jet impinging upon a normal plate with a ring slot penetration and on the right a diagram highlighting the boundary locations (1-4), the variable parameters (R_s and A_s), the asymptotic jet region (top), the asymptotic tine region (right), and the turning region (dashed arrow) of the free surface.

be given by $\Delta R = A_s/2R_s$. In a typical sprinkler head, slot penetrations in the deflector plate have some angular dependence. In the axisymmetric model suggested the discrete openings in the actual plate are smeared out uniformly with respect to the angular coordinate, θ, and the radial location and width of the smeared locations are chosen to match the last two parameters mentioned above. By assuming the flow pattern to be axially symmetric, some of the geometric effects induced by the details of the deflector plate geometry are lost, but the impact of the general geometry of slots is preserved. Figure 2.2(a) shows an image of an axisymmetric sprinkler and Fig.2.2(b) shows the definition of R_s and A_s for this general axisymmetric case.

The boundary conditions of $\phi(\vec{r}_s)$ and its normal gradient, $\hat{n} \cdot \nabla\phi(\vec{r}_s)$, appearing in Eq. 2.10, are independent of θ. All of the bounding surfaces are now figures of revolution, and the only quantities containing an angular dependence are the Green's function and its normal derivative.

The goal of a sheet formation model is to take the initial conditions of a sprin-

kler (the total flow, pressure, and geometry) and to produce the initial conditions for sheet breakup model (sheet location, velocity, and thickness). With the appropriate nondimensionalization the model can be reduced to solving for the sheet location, sheet trajectory angle, and sheet thickness. Here sheet initial location is found at the edge of the deflector, R_D for the tine sheet, and at the slot radius location, R_s for the slot sheet. Because we are assuming potential flow, the fluid sheet velocity magnitude is simply 1, and the only defining quantity for sheet velocity is sheet trajectory angle, θ_t and θ_s, for the tine and slot sheet respectively. The sheet thickness can be nondimensionalized, like the other quantities, as $T = T/R_j$, where nondimensional tine sheet thickness can be shown to be given by

$$T_t = \frac{1-\alpha}{2R_D}, \tag{2.15}$$

and slot sheet thickness by

$$T_s = \frac{\alpha}{2R_s}, \tag{2.16}$$

where α is the flow split, or the fraction of the total flow which pases through the deflector plate.

Figure 2.3 shows the general inputs and outputs of the sheet formation model, as well as the method of solution, in which pressure and flow split are iteratively solved for (explored in Sec. 3.1).

Before we begin exploring boundary conditions specific to the axisymmetric model, it is important to explore the assumptions implicit in this model. The ax-

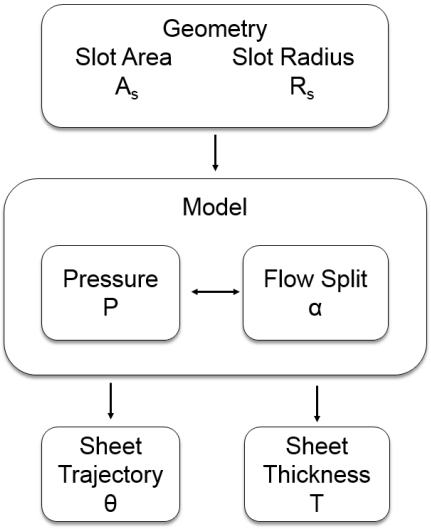

Figure 2.3: The sheet formation model transforms the sprinkler geometry, R_s and A_s, into sheet trajectory, θ_{traj} and thickness, T, the necessary inputs for the sheet breakup model.

isymmetric model itself extends infinitely in height and radial extent, and is suitable for a slot of any size. A true sprinkler does not. A true sprinkler has a finite deflector, and small regular slots. In order to implement our boundary conditions, the following assumptions about applicability must be made:

1. The deflector radius, R_D, must be sufficiently large so that fluid behavior can be treated as asymptotic.

2. The deflector radius, R_D, must be sufficiently small, so that viscous effects are minimal.

3. The slot width, ΔR, must be sufficiently small so that the small orifice approximation holds.

Condition 1 can be shown to be true through asymptotic analysis of the tine stream (Eq. 2.37) for $r > 2$. The validity of condition 2 has been previously outlined, and condition 3 will be explored in Sec. 2.4.

In order to outline the boundary conditions it is first neccesary to choose a suitable Green's function. Because we are examining an axisymmetric case, the only quantity that depends on angle is the Green's function. The axisymmetric Green's function can be achieved by angularly integrating the Green's function presented in Eq. 2.11. The result takes the form

$$\mathcal{G}\left(\vec{r},\, r_o,\, z_o\right) = -\frac{1}{4\pi}\int_0^{2\pi} \frac{1}{\sqrt{r^2 + r_o^2 - 2rr_o\cos(\theta - \theta_o) + (z - z_o)^2}}\, d\theta_o. \tag{2.17}$$

The quantity, $\mathcal{G}$, physically represents a ring source of fluid situated at $r = r_o$, $z = z_o$. The Green's function can then be rewritten as

$$\mathcal{G}\left(\vec{r},\, r_o,\, z_o\right) = -\frac{1}{\pi\sqrt{(r + r_o)^2 + (z - z_o)^2}}\int_0^{\pi/2}\left(1 - \frac{4rr_o}{(r + r_o)^2 + (z - z_o)^2}\,\sin^2(\theta)\right)^{-1/2} d\theta. \tag{2.18}$$

This function can be evaluated in terms of the complete Elliptic Integrals of the first kind, denoted as $K(m)$ where

$$K(m) = \int_0^{\pi/2}\left(1 - m\,\sin^2(\theta)\right)^{-1/2} d\theta. \tag{2.19}$$

The Green's function being rewritten as

$$\mathcal{G}\left(\vec{r},\, r_o,\, z_o\right) = -\frac{1}{\pi\sqrt{(r + r_o)^2 + (z - z_o)^2}}\, K\left(m\right) \tag{2.20}$$

where

$$m = \frac{4rr_o}{(r + r_o)^2 + (z - z_o)^2}. \tag{2.21}$$

This axisymmetric Green's function can again be refined by posing the no penetration condition at $z = 0$ as demonstrated in Eq. 2.12 with the form

$$\mathcal{G}_1(\vec{r},\, r_o,\, z_o) = \mathcal{G}(\vec{r},\, r_o,\, z_o) + \mathcal{G}(\vec{r},\, r_o,\, -z_o)\,. \tag{2.22}$$

Similar to $\mathcal{G}$, $\mathcal{G}_1$ represents a ring source situated at $r = r_o$, $z = z_o$ but located in a semi-infinite space bounded below by the plane $z = 0$. Figure 2.1 shows a plot of this Green's function and the streamlines generated from this Green's function ($\nabla\mathcal{G}_1$) with a source at $r_0 = 1.0$ and $z_0 = 0.5$.

The task now remains to define the boundary conditions. There are four bounding surfaces as shown in Fig. 2.2(b) and described as the

- Jet, an inlet disk of radius R_j located at a given height, Z_j;
- Free Surface, the bounding free streamline surface. This surface can be divided into three regions. The asymptotic jet free surface, the asymptotic tine stream free surface, and the turning region which connects the two;
- Tine Stream, a vertical cylinder of radius R_{ts} and height z_s (the vertical distance between the bounding free streamline and the deflector plate) where the flow that does not pass through the deflector plate exits;

- Deflector, the horizontal deflector plate where flow passes through the ring opening with centroid R_s and total area A_s.

2.3.1 Bounding Surfaces

Because of the formulation of the problem as a surface integral, each individual boundary can be evaluated individually, and summed to construct the entire integral as

$$\phi(\vec{r}) = \phi_j(\vec{r}) + \phi_{fs}(\vec{r}) + \phi_{ts}(\vec{r}) + \phi_d(\vec{r}), \tag{2.23}$$

where $\phi_j(\vec{r})$, $\phi_{fs}(\vec{r})$, $\phi_{ts}(\vec{r})$, and $\phi_d(\vec{r})$ correspond to the integral $\phi(\vec{r})$, as defined in Eq. 2.10, evaluated on the surface of the inlet jet, free stream, tine stream, and deflector plate, respectively. Because of the inviscid nature of the flow, the distance at which the inlet jet and the tine stream barriers are evaluated is arbitrary. At a sufficient distance from the deflector plate and the vertical axis, respectively, the flow on both of these boundaries converges to some asymptotic behavior.

The impinging jet can be imagined as a circular cylinder of radius R_j with a downward speed U_j extending to infinity. Thus, as $z \to \infty$, $\phi \to -U_j z$. Similarly, the deflector plate with the specified opening governed by R_s and A_s extends so it occupies the entire plane $z = 0$. The jet thickness then approaches 0 as $r \to \infty$. It is worth noting that all analytical solutions for free jet problems described in the literature are posed as infinite domain problems. This has not prevented their use in the study of problems in a finite domain.

It is helpful to construct a global mass balance to quantify how the flow enter-

ing through the inlet jet leaves the deflector. The inlet volume flow is dimensionally quantified as $\pi R_j^2 U_j$, or non dimensionally as simply π. A fraction, α, or the flow split, of this flow leaves the domain in the slot stream through one or more holes in the deflector plate. The remaining fraction, $1-\alpha$, is trapped between the surface of the deflector and the ambient air. Because the ambient pressure remains constant, the speed of the radially moving tine stream must also be U_j. Thus, if we let z denote the thickness of the tine stream, conservation of mass requires that

$$(1-\alpha)\pi R_j^2 U_j = 2\pi r z_s U_j, \tag{2.24}$$

or non-dimensionally,

$$r z_s = \frac{(1-\alpha)}{2}. \tag{2.25}$$

The shape of the of the asymptotic streamline leaving the deflector is then a hyperbola whose thickness is determined by the fraction of mass flow passing through the plate or the flow split. The flow split must be determined as a part of the solution to the problem.

2.3.1.1 Jet

Now considering the region $z \gg 1$ far from the deflector plate. The presence of the plate creates a perturbation that retards and expands the jet, deflecting the boundary in the process. The dimensionless potential at this jet boundary can be

represented as

$$\phi_{jet}(r,z) = -z + \Phi(r,z). \tag{2.26}$$

The appropriate boundary conditions for the perturbation potential, $\Phi(r,z)$ are

$$\lim \ \Phi(r, z \to \infty) = 0 \tag{2.27}$$

and

$$\left[\left(-1 + \frac{\partial \Phi}{\partial z}\right)^2 + \left(\frac{\partial \Phi}{\partial r}\right)^2\right] = 1. \tag{2.28}$$

The first condition requires that the perturbation to the jet flow vanish sufficiently far from the plate while the second arises from the requirement that the pressure and thus the jet speed be uniform at the jet free surface. Neglecting the quadratically small terms, the second condition can be simplified to the linearized form

$$\frac{\partial \Phi}{\partial z}(1,z) = 0. \tag{2.29}$$

From Eq.2.3 and the boundary conditions, Eqs. 2.27 and 2.29, any solution for $\Phi(r,z)$ can be written as

$$\Phi(r,z) = \sum A_n J_0(\lambda_n r) exp(-\lambda_n z) \tag{2.30}$$

where A_n are some series of undetermined constants, J_0 are the Bessel functions of

order zero and λ_n are a set of eigenvalues corresponding to the Bessel function such that $J_0(\lambda_n) = 0$. Because each subsequent eigenvalue increases by approximately π, the subsequent exponential terms can be shown to decrease by more than an order of magnitude, thus only the first term in the series above is important. As a result the asymptotic solution on the jet can now be completed.

The jet velocity normal to the jet boundary is given by the derivative of Eq. 2.30 with respect to z

$$v_{jet}(r,z) = \frac{\partial \Phi(r,z)}{\partial z} = -1 - A_0 \lambda_0 J_1(\lambda_0 r) exp(-\lambda_0 z) \tag{2.31}$$

and an asymptotic free streamline, or the free streamline which passes through the jet radius, $R_j = 1$, has the shape

$$r = 1 - A_0 J_1(\lambda_0) exp(-\lambda_0 z). \tag{2.32}$$

From the Eqs. 2.30 - 2.32, the boundary integral, $\phi_j(\vec{r})$, can now be evaluated at the inlet, a horizontal plane located a non-dimensional distance Z_j above the deflector plate.

$$\phi_j(r,z) = \int_0^{R_j} r_0(\phi_{jet}(r_0, Z_j)\mathcal{G}_1(\vec{r}, r_0, Z_j) - v_{jet}(r_0, Z_j)\frac{\partial \mathcal{G}_1(\vec{r}, r_0, Z_j)}{\partial z})dr_0 \tag{2.33}$$

2.3.1.2 Free Surface

The chief problem for the general solution to the proposed boundary value problem is selecting an appropriate shape for the free-surface boundary. An approximation of the surface as a combination of hyperbolas is a reasonable one for the axisymmetric ring slot case. Using the criteria that the non-dimensional free surface must approach $r = 1$ as $z \to \infty$ and $z(r) = (1 - \alpha)/2r$ as $r \to \infty$ the free-surface can be approximated as

$$z = f(r) = \frac{A}{1 - r} + \frac{B}{r}. \tag{2.34}$$

where A and B are constants chosen for continuity with the jet and tine stream boundaries.

Assessing the boundary integral, $\phi_{fs}(\vec{r})$, is simplified greatly by the requirement that there is no normal flow to the free-surface. The fluid potential on the surface increases linearly with arclength, because the magnitude of the speed in the tangential direction is always 1. The integral is assessed from $r_0 = 1$, or the radius of the jet, to $r_0 = R_{ts}$, or the arbitrary location of the tine stream boundary, along the curve bounded by the free-surface equation given in Eq. 2.34. $\phi_{fs}(\vec{r})$ can be written as

$$\phi_{fs}(\vec{r}) = \int_1^{R_{ts}} r_0 \phi(r_0, f(r_0)) \frac{\partial \mathcal{G}_1(\vec{r}, r_0, f(r_0))}{\partial n} dr_0 \tag{2.35}$$

where $\partial \mathcal{G}_1 / \partial n$ can be found by the following

$$\partial \mathcal{G}_1 / \partial n = \nabla \mathcal{G}_1 \cdot \hat{n} \tag{2.36}$$

where $\hat{n}$ is the unit normal to the free-surface at any given r_0, and $\mathcal{G}_1$ is given by Eq. 2.22.

2.3.1.3 Tine Stream

The impact of the next boundary, $\phi_{ts}(\vec{r})$, is now considered. In the region near the plate, $r \gg 1$, as $r \to \infty$, the radially expanding jet thins. Since the speed of the jet is fixed by the requirement of constant pressure, the limiting form of the solution for large r must be $\phi \to U_j r$, as shown by Eq. 2.24. This is not, however, a solution for an axisymmetric fluid potential, given in Eq. 2.14. The requirement given by Eq. 2.24 can be satisfied by posing the solution to the axisymmetric fluid potential in this region as a descending series, with the leading term, r. The solution for the velocity potential in this region takes the form of an infinite series

$$\phi_{tine}(r, z) = r + F_1(z)/r + F_2(z)/r^3 + ... \tag{2.37}$$

where $F_1(z)$ and $F_2(z)$ are functions which are chosen to satisfy Eq. 2.14 and the free surface boundary conditions. Enforcing the boundary condition that as the tine stream moves radially outward vertical velocity tends to zero, or $v(r, 0) = 0$, gives

$$F_1(z) = -z^2/2! + c \;\text{ and }\; F_2(z) = z^4/4! + d. \tag{2.38}$$

Note that this form of the solution restricts its validity to a region of r greater than the radial location of the slot in the deflector plate. The above constants c

and d are determined from the requirement that the speed is constant at the free surface. To accomplish this, the equation for the free surface must also be expanded into a descending series in r as

$$z(r) = (1-\alpha)/2r + b/r^3 + ... \tag{2.39}$$

This introduces another constant, b. The solution for ϕ_{tine} given by Eq. 2.37 must also be made consistent with the shape of the free surface. The results yield that $b = c = 0$ and $d = -(1-\alpha)^2/4$. This result holds no matter what fraction of the mass flow passes through the plate, subject to the caveat that the domain of applicability lies outside the opening in the plate.

This boundary is evaluated at the arbitrary radius of the plate, $r_0 = R_{ts}$, with the integral spanning $0 < z_0 < z_s$, where z_s is the height of the sheet above the deflector plate given by $z\left(R_{ts}\right)$ from Eq. 2.39.

$$\phi_{ts}(r,z) = \int_0^{z_s} r_0(\phi_{tine}(R_{ts},z_0)\mathcal{G}_1(\vec{r},R_{ts},z_0) - v_{jet}(R_{ts},z_0)\frac{\partial \mathcal{G}_1(\vec{r},R_{ts},z_0)}{\partial z})dz_0 \tag{2.40}$$

2.3.1.4 Deflector

The final boundary, the deflector, is evaluated at $z_0 = 0$ and spans $0 < r_0 < R_{ts}$. Because of the choice of Green's function, $\partial\mathcal{G}_1/\partial n$ is equal to 0 at all $z = 0$. The term, $\partial\phi/\partial n$ is also equal to 0 at all points where there is no penetration through

the boundary. As a result, the integral, $\phi_d(\vec{r})$, can be written as

$$\phi_d(\vec{r}) = \int_0^{R_{ts}} r_0 v(r_0, 0) \mathcal{G}_1(\vec{r}, r_0, 0) dr_0, \tag{2.41}$$

where $v(r_0)$ is the profile of flow through the ring opening with centroid R_s and total area A_s. This flow profile can be assessed based upon the typical results of 2D slot flow, discussed in section 2.4. Using the static pressure at the location of the slot as calculated from Bernoulli's equation in Eq. 2.4, a total slot flow, $v(r_0, 0)$, can be determined.

The above integrals can be summed following Eq. 2.23 to calculate the full potential $\phi(\vec{r})$ and the corresponding flow split, α. From α, the sheet thicknesses, T_T and T_S, and trajectories, θ_T and θ_S, can be determined.

2.4 Slot Flow

The flow through the deflector plate, or the slot flow, is an important component in the picture of total flow. A challenge is predicting how much of the total flow passes through a slot. When exiting a slot, the velocity of the free streamlines bounding the slot stream can be found from Bernoulli's equation, as given in Eq. 2.4.

The free surface of the slot stream must have a gauge pressure of 0, or a velocity magnitude equal to the velocity magnitude of the jet free surface. The velocity normal to the slot, $v(R_s, 0)$, can than be calculated from the horizontal velocity at the slot, $u(R_s, 0)$, as

$$v(R_s, 0) = \sqrt{1 - u(R_s, 0)^2}. \tag{2.42}$$

Because the exit is not a smooth, well contoured nozzle, but rather a flat plate, the width of the slot stream will be less than the width of the slot opening. This vena contracta effect is a result of the inability of the fluid to turn the sharp corner of the flow [3]. Because the streamlines in the exit plane are curved the pressure across them is not constant. We are not interested in the details of this flow pattern, but only total flow through the slot. The assumption of a uniform velocity with straight streamlines are not valid at the exit plane, but are valid in the plane of the vena contracta [24].

A flow coefficient, C_d, can be used to calculate the ratio between the idealized mass flow, $\dot{m}_i$, given by Bernoulli, and the actual mass flow through a slot, $\dot{m}_a$, as

$$C_d = \frac{\dot{m}_a}{\dot{m}_i}. \tag{2.43}$$

In general a flow coefficient accounts for all of the physics not included in the ideal flow model; for example, contraction, turbulence, and viscous effects. The value of C_d is well explored for the case of a small slot, as in the case of an orifice plate. In Leinhard [24] this value is given as

$$C_d = \frac{\pi}{\pi + 2}. \tag{2.44}$$

This is the slot coefficient for small, sharp edged orifices. For an orifice plate,

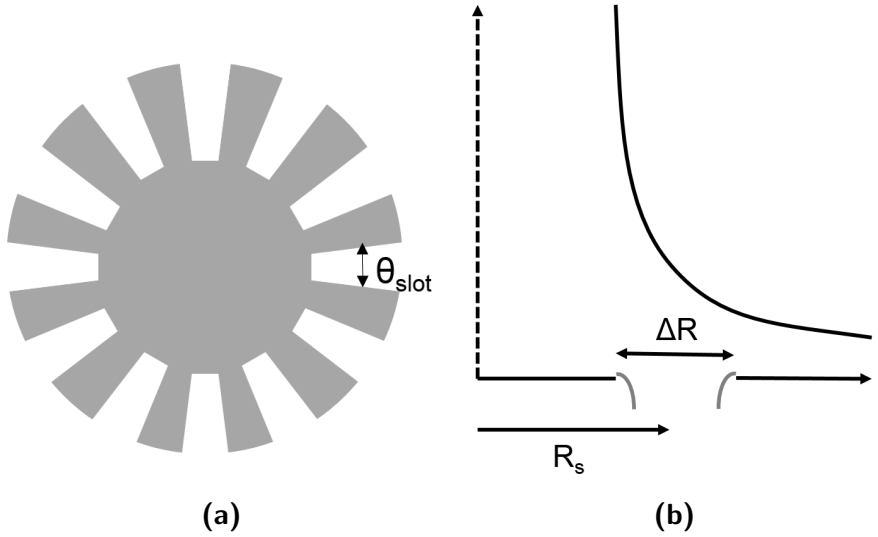

Figure 2.4: In order for the small slot flow assumptions to hold the size of the orifice must be much less than 1. In a typical sprinkler(a) this corresponds to requiring that $\theta_{slot}/2\pi \ll 1$, where θ_{slot} is the angular extent of a single slot and for the axisymmetric sprinkler(b) requiring $\Delta R/R_s \ll 1$.

this requirement is given by $R_o/R_j \ll 1$, where R_o is the radius of the orifice and R_j is the radius of the flow approaching the orifice [24]. An analogy can be made for a standard sprinkler by requiring that $\theta_{slot}/2\pi \ll 1$, where θ_{slot} is the angular extent of a single slot and similarly to the case of the axisymmetric sprinkler by requiring $\Delta R/R_s \ll 1$. Figure 2.4(a) shows a typical sprinkler and 2.4(b) the axisymmetric sprinkler meeting the narrow slot requirement.

This requirement, and the definition of ΔR, limits the choice of sprinkler geometries to any situation where

$$\frac{A_s}{2R_s^2} \ll 1. \tag{2.45}$$

.

Total flow through the slot can than be approximated as flow of a uniform

velocity, as given by Eq. 2.42. Ideal mass flow through the slot is simply

$$\dot{m}_i = \rho A_s v(R_s, 0), \tag{2.46}$$

where ρ is the fluid density, A_s is the slot area, and the velocity normal to the slot opening, $v(R_s, 0)$, as given by Eq.2.42. Actual flow, as given by Eq. 2.43, is then

$$\dot{m}_a = C_d \rho A_s v(R_s, 0). \tag{2.47}$$

In the non-dimensional formulation, the total mass flow is simply $U_j A_j = 1$. The flow split is then given as

$$\alpha = C_d A_s v(R_s, 0). \tag{2.48}$$

The next task is to discuss the implementation of the model.

Chapter 3: Modeling Implementation

The mathematical model outlined in the above chapter is quite general and even with the simplifying assumptions has no analytic solution. Even the much narrower axisymmetric model with asymptotic boundary conditions has no analytical solution and relies on a numerical solution to calculate the result. Early research by Schach, who outlined a similar potential model of a jet impinging on a deflector with no slot, stated that there was no way for the integrals posed to be solved [16] . Fortunately, there have been tremendous advancements in computational power and formulations. The following chapter outlines the methodology by which the integral equations of the preceding mathematical model were solved. Additionally, some of the techniques for verifying the performance of the model and assessing error, both numerical and otherwise, are outlined.

3.1 Computation

The solution of the axisymmetric model outlined in section 2.3 relies on the summing of the integrals constructed from the boundary conditions of the potential flow and a Green's function chosen to be representative of a source within the problem's constraints. However, the full details of the boundary conditions of the

potential flow are not known. In particular, it is impossible to know a priori the shape of the free surface, the height of the tine stream, or the static pressure which drives and determines flow through the slot. It is possible, however, to approximate a general form for these boundary conditions which can vary based upon a specific parameter.

For calculations performed within this thesis the parameter chosen was α, the flow split, or the ratio of flow through the deflector to total flow. Figure 2.2 outlines the boundaries that are integrated over and the regions of the flow. The asymptotic jet boundary and the jet free surface boundary, or the portion of the free surface distant from the deflector plate, are independent of flow split. For a given flow split the height of the tine stream is precisely specified and thus the asymptotic tine stream boundary and the tine stream free surface are also completely determined. The turning region free surface, or the region of the free surface which connects the jet free surface and the tine stream free surface, is assumed to be a hyperbola with end points corresponding to the interior ends of the jet free surface and the tine free surface, and is thus also determined from a specified flow split. The only remaining boundary is the deflector plate boundary. The only information necessary for the solution of the deflector plate boundary is the velocity above the slot. This however cannot be known without first solving for the full potential by summing the integrals above, which includes the integral along the deflector plate boundary. Additionally, the flow split necessary for the other boundaries is, in turn, determined by the total flow through the deflector plate.

The solution to this problem is an iterative solution method. Figure 3.1 con-

tains a flow chart which outlines the simplified iterative process by which the correct potential flow can be solved for. First, the general parameters of the problem, such as slot area and slot radius are specified. A flow split is than approximated, and used to inform the boundary integrals. Next the appropriate Green's function and gradients are specified. The boundary integrals are then numerically solved to yield the velocity on the plate. This velocity, coupled with a slot flow coefficient and slot area allows for the calculation of flow through the slot and thus the calculation of a new flow split. This flow split then can be used to inform the boundary integrals again. This process repeats until a convergence is reached.

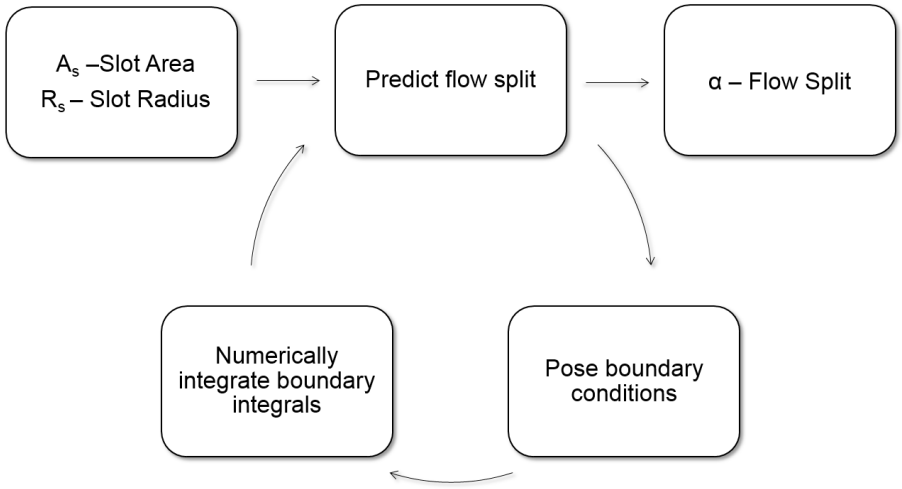

Figure 3.1: A simplified rendering of the iterative process used to converge upon the true flow split and potential flow for a given slot configuration (A_s and R_s).

The result is a potential flow corresponding to a specific axisymmetric scenario with given slot radius and area. The calculations performed in this thesis were performed using Wolfram Mathematica. Each boundary integral was calculated using the NIntegrate function, with specified option of AccuracyGoal = 3, and

using the Automatic method with SymbolicProcessing=0. NIntegrate is a built in function within the Mathematica framework which numerically integrates a specified integral. These methods were chosen to strike a balance between calculation speed and overall accuracy. The justification for these choices is explored in section 3.3.

3.2 Error Assessment

The results calculated using the model above are for an idealized sprinkler: a sprinkler completely following potential flow models without the effects of turbulence or viscosity, one that does not allow for atomization (on the sprinkler deflector itself), and one that does not correspond to to any existing sprinkler. There are three possible sources of error in a model such as this. First, errors in the assumptions of the model relative to the reality of the situation. These errors would be found through comparison with experiment. Because there is no existing sprinkler with this ideal geometry described, validation of the model has not been performed. Second, there are numerical errors associated with numerically evaluating integrals in the way proposed. Lastly, there is the error introduced by the assumption of the location of the free surface or of other boundary conditions.This last error is most likely to manifest in errors of speed along the free surface boundary.

3.2.1 Experimental Error

Some experimental data does in fact exist which explores an axisymmetric jet impinging upon a normal deflector plate. Experiments performed by Labus [25]

measured the shape of the free surface of an impinging jet. The experiments were quite limited in scope however, and do not contain any information regarding the cases of interest for our experiments, namely the cases where some fraction of the flow passes through the deflector plate. These results can be compared to the trivial solution where the flow split, $\alpha = 0$, but do not provide much insight into the accuracy of the model in the general case.

Figure 3.2 show the experimental data compared to the predicted solution for the case mentioned above. Qualitatively strong agreement is seen and a mean percentage difference of 5.3% can be calculated between the experimental and predicted data points. We can expect errors associated with the free surface speed to be of a comparable magnitude, between 5 - 15%.

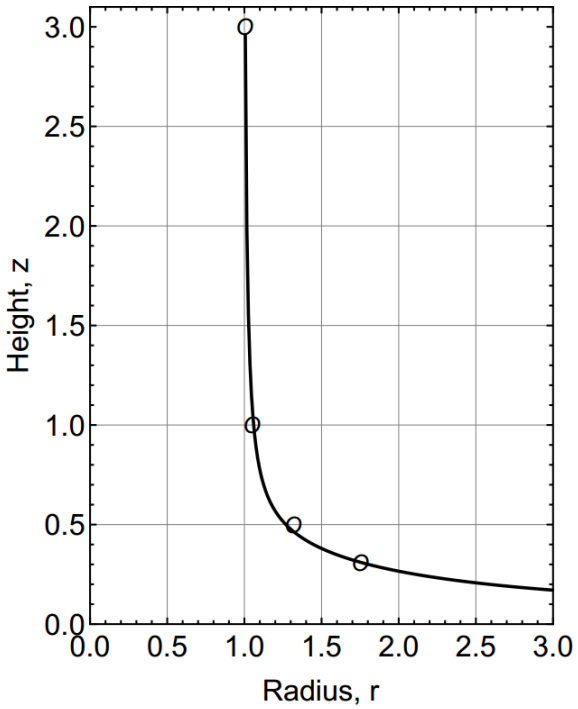

Figure 3.2: The experimental data (circles) taken by Labus [25] closely coincides with the predicted free surface shape for the $\alpha = 0$ case, with a mean percentage difference of 5.3%.

3.2.2 Numerical Error

Assessment of the numerical error can be performed through direct comparison of specified fluid potential to calculated fluid potential. This direct comparison method is available in known solutions, namely the limited examples of the asymptotic tine and asymptotic jet boundaries. By constructing a boundary integral around the asymptotic jet or asymptotic tine region, and comparing calculated fluid potential to known fluid potential, the accuracy of the model can be assessed. These boundary integrals can be considered about the shaded regions indicated in Fig. 2.2. Potential error is given as

$$\epsilon = \left| \frac{\phi_{calc.} - \phi_{true}}{\phi_{true}} \right| \tag{3.1}$$

where $\phi_{calc.}$ is the calculated fluid potential and ϕ_{true} is the specified fluid potential.

Figure 3.3 shows error, ϵ, as well as velocity error, ϵ_v, mentioned in the following section, at a number of points along the centerline of the asymptotic regions. The velocity potential method of error assessment shows a very low mean error, on the order of 10^{-5}. This error can be taken as the numerical error inherent in the method. It is important to note that the error increases dramatically at the boundaries themselves as the boundaries are singularities. The low mean value of error provides verification of the codes ability to evaluate the numerically posed integrals. Figure 3.4 show the potential flow over a narrow region of the asymptotic jet (a) and asymptotic tine sheet (b).

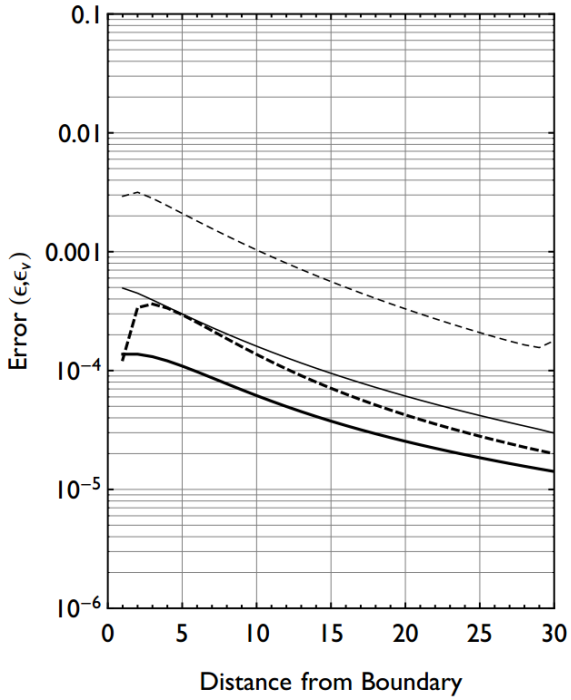

Figure 3.3: The potential error ϵ for the asymptotic jet (thick solid) and asymptotic tine sheet (thin solid) as well as the free surface velocity error, ϵ_v, for the asymptotic jet(thick dashed) and asymptotic tine sheet (thin dashed) for a number of points with increasing distance from the boundary singularity.

3.2.3 Free Surface Speed

In addition to direct comparison of fluid potential, other outputs of the model can be compared with expected values. The potential flow model necessitates that the free streamline bounding the upper layer of the water flow must have a constant velocity magnitude of one. Because the true value of this velocity magnitude is known, and the velocity magnitude in calculated results can be found, this becomes the most promising candidate for a general method of assessing model error.

It is important to note however that error calculated based upon the free surface speed will in almost all cases be greater than the error in the velocity potential

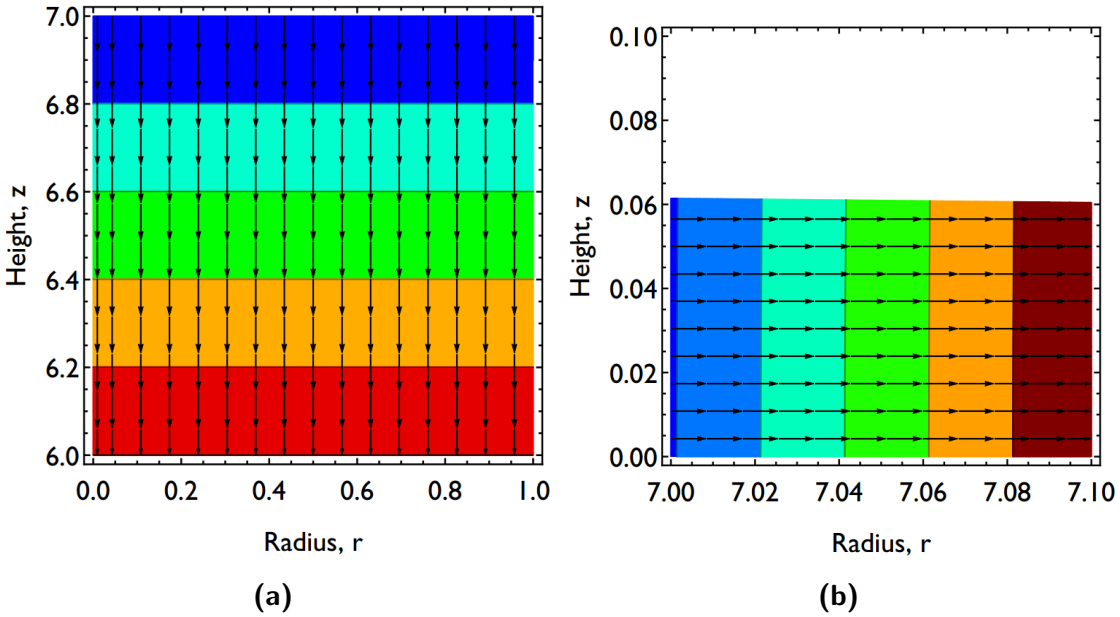

Figure 3.4: The asymptotic potential in the Jet (a) and Tine Sheet (b) can be numerically solved for in the same way as the global axisymmetric solution. Error of this numerical solution can be seen in Fig. 3.3.

as a result of error propagation through the derivative of the velocity function. Here error can be assessed locally, or as a mean error for the entire free surface.

The velocity error can be given by

$$\epsilon_v = \left| \frac{\sqrt{u^2 + v^2} - 1}{1} \right| \tag{3.2}$$

where u and v are the non-dimensional velocities in the r and z directions, respectively.

Figure 3.3 shows a plot of the true error and velocity error near the free surface for a number of points along the length of the free surface for both the asymptotic jet and asymptotic tine stream regions. It can be seen that the velocity error is substantially higher than the potential error in all cases, on the order of 10^{-3}.

Because this error is calculated for a known case, where all the boundary

conditions are fully understood, it can also be viewed as a numerical error associated with the model. Error assessment of the results presented in the next chapter were performed using the velocity error method.

3.3 Numerical Strategies

The problem as stated uses the sum of several integrals over an infinite domain to calculate the value of some arbitrary point within that domain. Unfortunately, these integrals do not have an explicit solution and must be solved numerically. Further, in order to complete the boundary integral by summing over the entire domain, the two far boundaries of the jet and tine stream (at $r = R_{ts}$ and $z = Z_j$), must be solved for at a finite distance. The goal while making these approximations is to minimize overall error.

First, because the integrals must be solved numerically, the numerical integration scheme must be chosen appropriately. Mathematica's NIntegrate function offers a number of adaptive and non-adaptve schemes. Figure 3.5 shows the true error in the asymptotic jet case for three integration strategies, "Global Adaptive", "Monte Carlo", and "Trapezoidal". "GlobalAdaptive" reaches the required precision and accuracy goals of the integral estimate by the recursive bisection of the subregion with the largest error estimate into two halves and computes the integral for each half. Mathematica's default integration strategy, "Global Adaptive", shows far and away the lowest error, and is the integration strategy chosen for the work performed in this thesis. A global adaptive strategy reaches the required precision

and accuracy goals of the integral estimate by recursive bisection of the subregion with the largest error estimate into two halves, and computes integral and error estimates for each half.

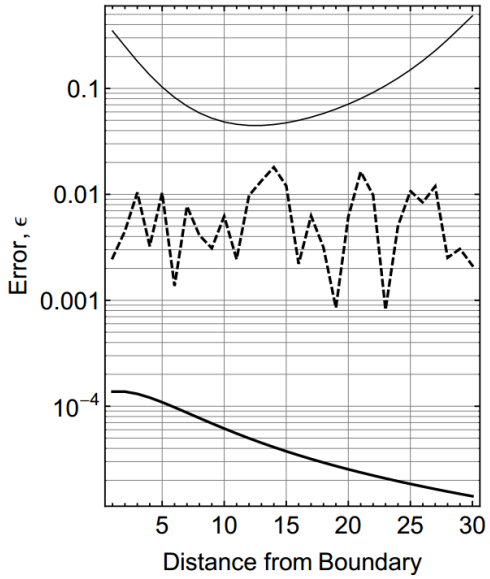

Figure 3.5: The true error in the asymptotic jet region for "Global Adaptive" (thick solid), "MonteCarloRule" (thick dashed), and "Trapezoidal" (thin solid) integration methods in Mathematica's NIntegrate function.

The other source of potential error to consider is the impact of the location of our jet and tine sheet boundaries (at $z = Z_j$ and $r = R_{ts}$) as well as the width of our asymptotic regions. Figure 3.6 shows the posistion of the bounding surfaces for the asymptotic regions spanning in the jet from $\chi Z_j < z < Z_j$ and in the tine sheet from $\chi R_{ts} < r < R_{ts}$, where χ is some fraction which defines turning region span. The boundaries are thus as follows. The asymptotic jet boundary exists at $z = Z_j$. The asymptotic jet free surface from $\chi Z_j < z < Z_j$. The turning region free surface spans from $z = \chi * Z_j$ to $r = \chi * R_{ts}$. The asymptotic tine sheet free surface spans from $\chi R_{ts} < r < R_{ts}$. The asymptotic tine sheet exists at $r = R_{ts}$.

Lastly, the deflector boundary spans from $0 < r < R_{ts}$.

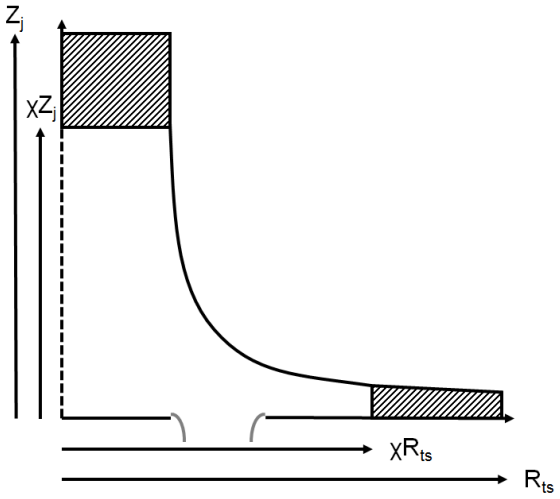

Figure 3.6: The asymptotic region definitions adapted from Fig 2.2(b) incorporating the parameter χ which scales the span of the turning region of the free surface.

Figure 3.7 shows the mean of the velocity error (Eq. 3.2) for a number of cases for a number of values of Z_j and R_{ts}(a) and χ(b). As a result of these calculations, the values of $Z_j = R_{ts} = 10.0$ and $\chi = 0.6$ were chosen because they produced the minimum average error. The optimum posistioning here suggests that there exists an ideal balance between when the asymptotic assumptions hold and when the turning region assumptions hold. This discussion is continued further in section 4.3.

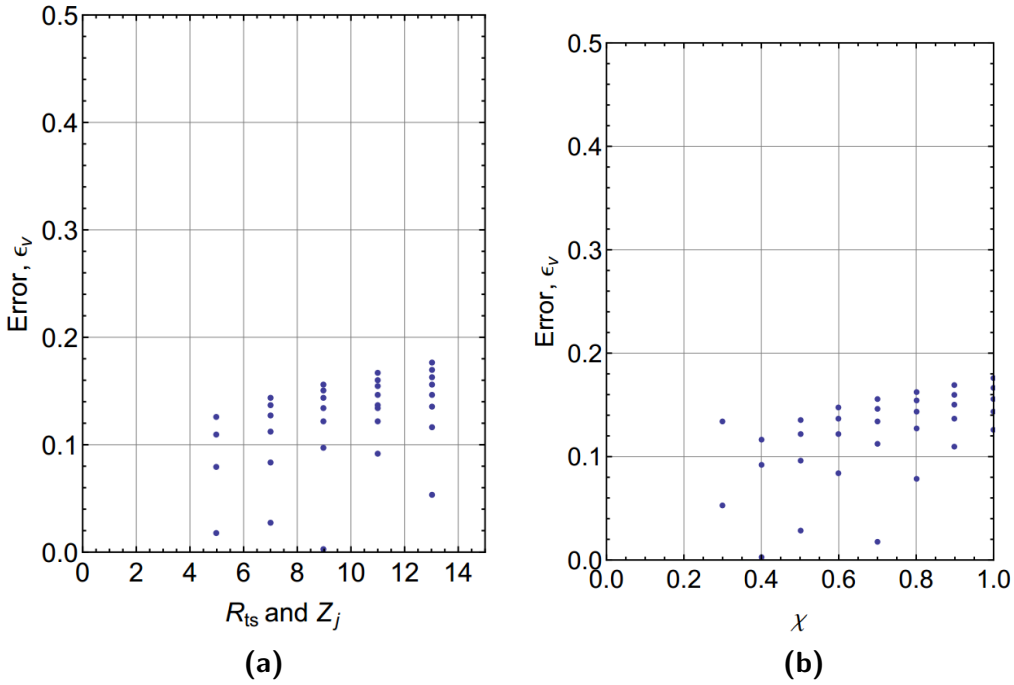

Figure 3.7: Mean velocity error for a number of slot configurations for varying values of $Z_j = R_{ts}$(a) and χ(b). The combination with the lowest overall error is chosen for numerical calculations

Chapter 4: Modeling Results

The following chapter contains the predictions made using the axisymmetric deflector model outlined in the preceding chapters as well as an error analysis and justification for the chosen parameters. The result of of calculating a potential flow for a given set of slot/deflector condition is a complete picture of the flow field on this deflector. Figure 4.1(a) shows a non-dimensional contour plot of fluid potential and streamlines over a narrow region near the deflector and the impinging jet. The potential shown is for the case where $A_s = 0.0$ with a resulting flow split of $\alpha = 0.0$ or a case in which no flow passes through the plate. Figure 4.1(b) highlights the change in the dominant feature of the potential flow, the free surface shape, and the dependence upon flow split, α. The shape of the free surface is the dominant feature in determining pressure along the plate, and thus total flow through a slot of a given configuration. Figure 4.2 shows the full fluid potential and streamlines over the bounds on integration for an axisymmetric case with no slot. It should be noted here that the asymptotic regions extend from $r = 6$ to $r = 10$ and from $z = 6$ to $z = 10$, and the turning region stretches between these two portions. The choice of the value $Z_j = R_{ts} = 10$ and $\chi = 0.6$ is explored in Sec. 3.3.

The potential flow results are dependent entirely upon the configuration of the

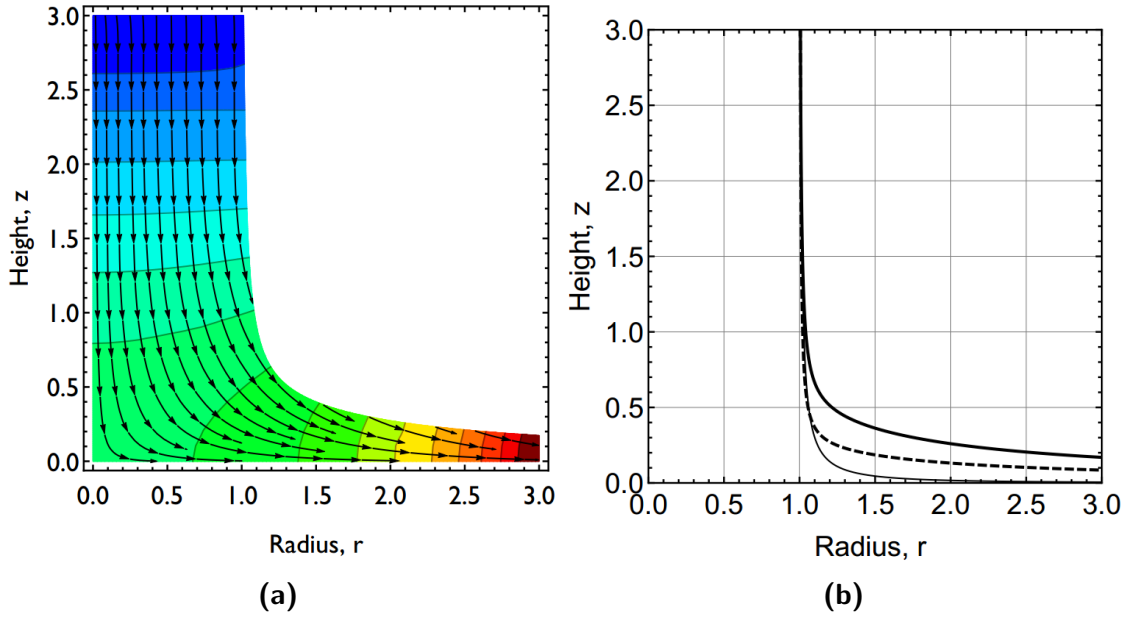

Figure 4.1: Contour plot of non-dimensional fluid potential and stream lines for an axisymmetric deflector (a) and free surface shape for $\alpha = 0.0, 0.5$, and 1.0 (b), respectively, from top to bottom.

slot, or the non-dimensional values of A_s and R_s.

4.1 Flow Split Predictions

The flow split, α, has been mentioned a number of times throughout this thesis but its importance bares reiterating. To begin, the flow split is among the most telling individual numbers when we discuss characterization of a sprinkler head. The flow split is the fraction of water which passes through the deflector relative to the total flow of the deflector. Put another way, the flow split characterizes the fraction of water that is thrown "mostly downward", the water that makes up the bulk of a sprinklers momentum, and the water delivered to the protected space immediately beneath the sprinkler head. The complement of the flow split, $(1-\alpha)$, in turn characterizes the water that is thrown outward, the fraction of the flow which

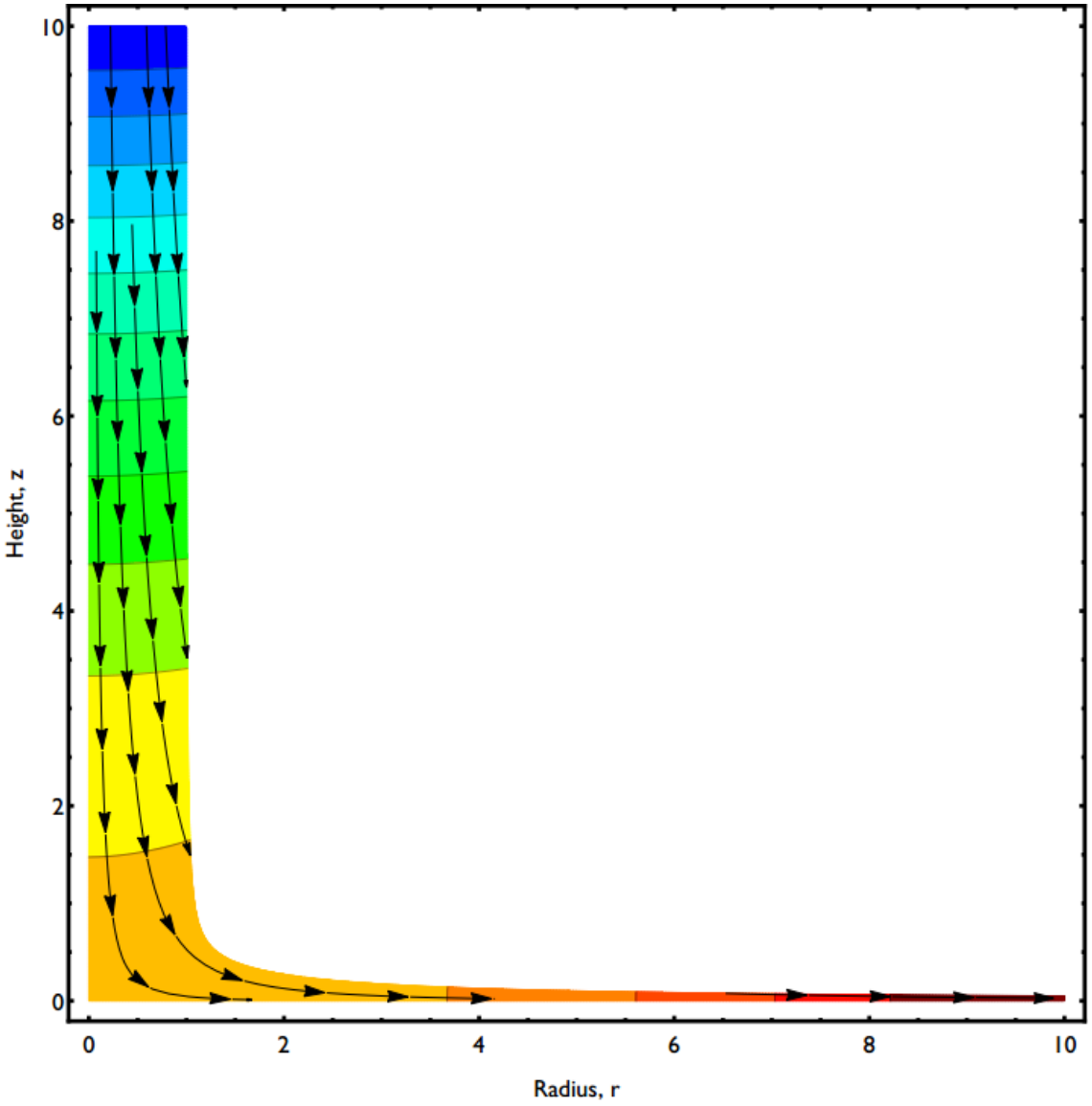

Figure 4.2: Contour plot of non-dimensional fluid potential and stream lines for an axisymmetric deflector with no slot ($\alpha = 0.0$). The asymptotic region extend from $r = 6$ to $r = 10$ and from $z = 6$ to $z = 10$, and the turning region stretches between these two portions .

does little for a sprinklers total momentum, and the water that is spread to cover the full range of the sprinkler spray. In a simplistic deflector, such as the axisymmetric sprinkler that has been discussed, the flow split (paired with the total flow rate and orifice size) is enough to completely characterize the sheet thickness and velocity for the fluid sheets leaving the deflector. This information in turn is sufficient to

predict drop size, drop distribution [2], and in effect all of the information necessary to completely characterize sprinkler spray.

Further, flow split is the number we have iterated over, and converged upon, within our axisymmetric model. It makes sense then to look at the impact of flow split on our model and the impact of the model parameters on the calculated flow split. The axisymmetric model allows slot parameters to be changed and explores the impact of R_s, the slot radius and A_s, the slot area. Figure 4.3(b) shows the impact of varying these parameters on flow split. It can be observed that as the area of the slot increases, so too does the flow split. This is expected as a greater portion of the slot is capable of flowing through a larger gap. As the slot radius increases the flow split decreases, meaning a greater portion of the flow is deflected by the deflector. When we look at the static pressure, p_s, along the deflector plate, as in Fig. 4.3(a), this too makes sense. Figure 4.3(a) shows the non-dimensional static pressure (a maximum value of 1) at the deflector plate vs. radius for flat plate with no slot. As we move radially outwards along the deflector plate we see the static pressure, or the ability of the flow to force flow through the slot, decreases.

These resultant dependencies provide insight into the impact of these two critical parameters, area and radius of the slots, on the performance of a sprinkler head. Further insight can be gained by examining the formula for calculating the flow split. Flow split, $\alpha = C_d v_{slot} A_s$. C_d is a function of the small slot assumption, and is always a constant value of approximately 0.61. The area of the slot, A_s, serves as an additional weighting factor. The normal velocity to the slot, v_{slot}, is determined entirely by the location of the slot geometry. Because of the small

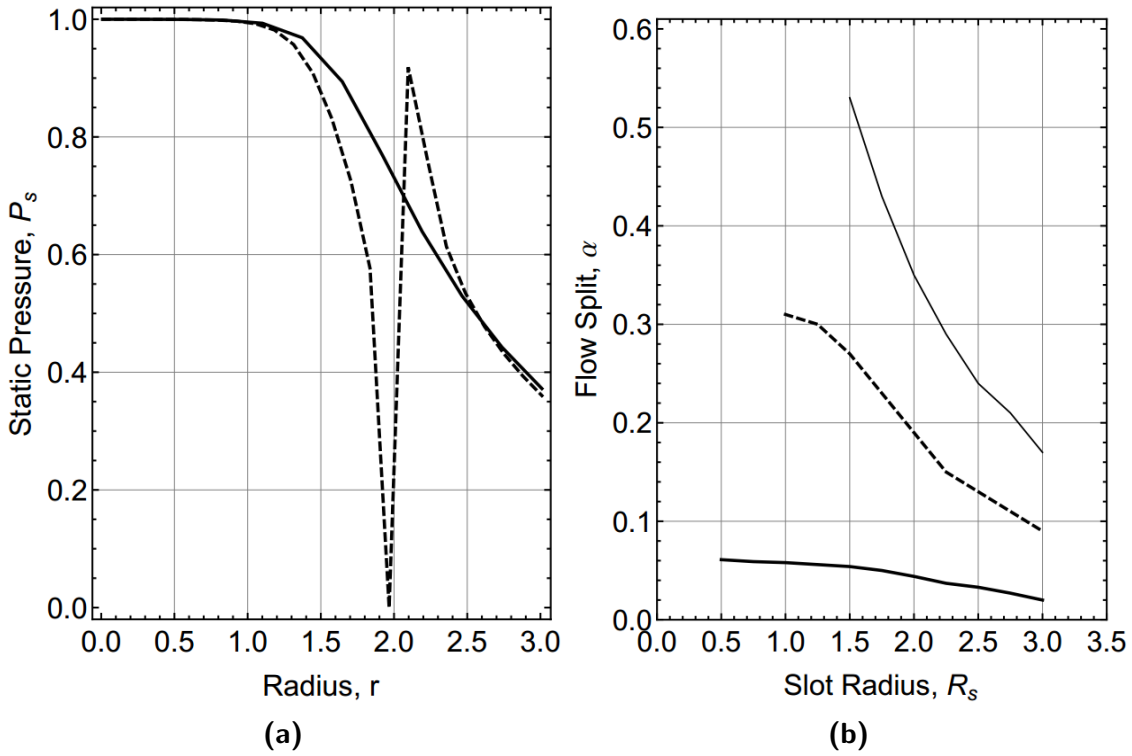

Figure 4.3: The calculated static pressure along the plate (a) for a case with no slot (solid line) and a slot at $R_s = 2$ (dashed line) and the flow splits resulting from various slot configurations (b) with $A_s = 1.0, 0.5$, and 0.1, respectively from top to bottom.

slot assumptions, v_{slot} is not change dramatically for differing slot areas. This can be seen in Fig. 4.4, which shows the flow split normalized by area for the three different slot areas. The flow split for any given slot radius, R_s, is approximately equal regardless of slot area, A_s. Slot normal velocity, v_{slot}, must range between 0 and 1, within the non-dimensional formulation. Consequently, flow split is bounded between 0 and $C_d A_s$.

4.2 Fluid Sheet Predictions

The key output of the sheet formation model are the thicknesses and trajectories of the tine and slot sheets. These quantities provide the necessary input to the

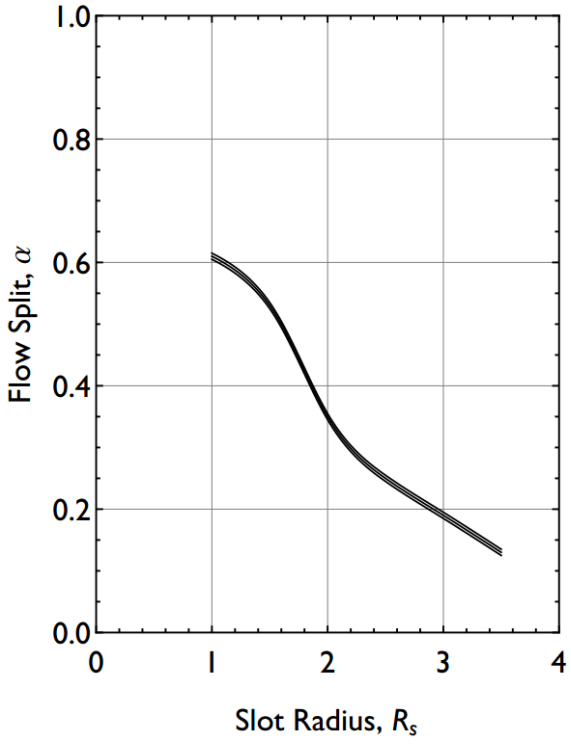

Figure 4.4: The calculated value of flow split, α, normalized by slot area, A_s, with each curve representing different slot areas. Because $\alpha = C_d v_{slot} A_s$, and v_{slot} must vary between 0 and 1, the flow split normalized by slot area varies between 0 and C_d.

sheet breakup and fragment transport model which serve to describe the remainder of the sprinkler behavior. Equations 2.15 and 2.16 describe the thickness of the tine sheet and the slot sheet, respectively.

Figure 4.5 shows the behavior of the slot and tine sheet relative to slot radius, R_s, and deflector radius, R_D, respectively, for a few flow splits.Slot sheets are shown in black while tine sheets are shown in red. The thick line, the dashed line, and the thin line correspond to flow splits of $\alpha = 0.2$, 0.4, and 0.6, respectively. Figure 4.5a shows the behavior of the sheet thicknesses, T_s and T_t. For both slot and tine sheet sheet thickness decreases with increasing slot and deflector plate radius. As flow split, α, increases, the slot sheet thickness increases and the tine sheet thickness

decreases. Figure 4.5b shows the behavior of sheet trajectory, θ_s and θ_t. For the slot sheets, sheet trajectory is the same regardless of flow split. These trajectories vary from 155° measured from the north pole of the sprinkler to 115°. The tine sheet trajectories are at much more shallow angles relative to the plate, all only slightly more than 90°, or approximately horizontal.

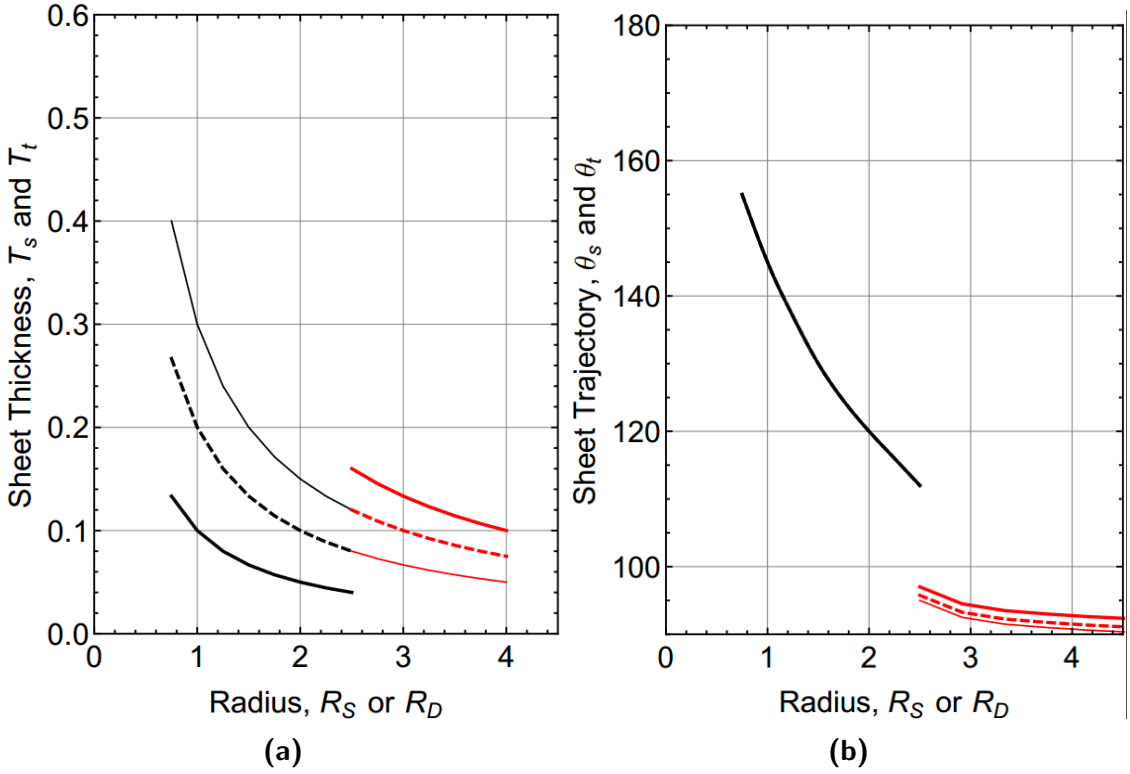

Figure 4.5: The slot and tine sheet relative to slot radius, R_s, and deflector radius, R_D, respectively, for a few flow splits.Slot sheets are shown in black while tine sheets are shown in red. The thick line, the dashed line, and the thin line correspond to flow splits of $\alpha = 0.2$, 0.4, and 0.6, respectively.

4.3 Error

Assessing the error in the model presented is a slight challenge, as discussed in section 3.2. It is obvious from visual inspection of the potential flow and the stream

lines in Fig. 4.1(a) that there are some minor errors. In the figure there are stream lines that cross in and out of the free surface, indication of an incorrect free surface shape. The direct measurement of this error is not available in the full axisymmetric mode because the exact potential function of the flow is the same unknown we are solving for.

The alternate method of error assessment that we instead turn to is the magnitude of error in the free stream velocity magnitude. This error is calculated at a number of points using equation 3.2 and is then presented as a mean value representing an approximated average error for the particular case. Figure 4.6 show the mean error calculated in this manor for a number of calculated cases, and is compared to the flow split. The mean error for all of the cases is approximately 7%, in the range predicted suggested earlier stemming from free surface shape.

There are a number of potential sources of error in the axisymmetric model. Numerical error inherent in the numerical calculation of the integrals was discussed in section 3.2 and is substantially smaller than the value of error calculated above. As a result, it is reasonable to attribute the error not to the numerical solution method, but rather to errors in the specified boundary conditions.

The most likely candidate is the shape of the free surface. This is the boundary condition about which we have the least information and which has the strongest impact on the total potential behavior. Figure 3.2 also highlights the discrepancy between the prescribed and experimentally calculate free-surface shape. This error is minor, but has a mean error on the same order as the error calculated in all cases using the free stream velocity magnitude method.

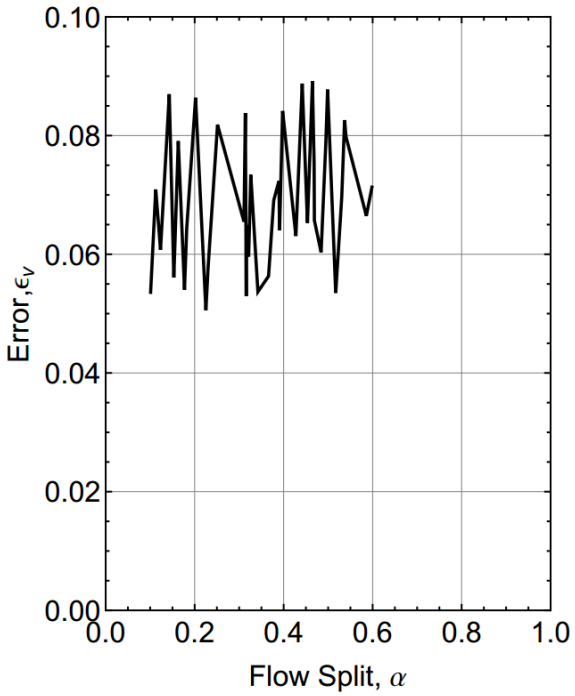

Figure 4.6: The calculated value of error along the free surface vs the flow split for a number of axisymmetric cases.

Another potential source of error stems from the slot flow coefficients. The small slot assumptions break down in limiting cases, and may cause predicted flow splits to differ from true flow splits.

A last source of error comes from the break down of the asymptotic tine sheet solution in extreme cases. For cases of low flow split, where most of the water does not pass through the plate, we would expect the tine sheet to converge upon its asymptotic behavior only at very large radii.

On the whole, the error calculated in this manner is minor. A true error, or deviation from actual behavior, requires experimental validation. A summary of, the implications of, and future work for, this model follow.

Chapter 5: Conclusions and Future Work

The mathematical model presented above provides a method for determining the free surface flow field on a perforated deflector plate. By posing the flow impinging on the sprinkler as a potential flow boundary value problem, and applying appropriate boundary conditions and selected Green's functions, the fluid-gas interface location can be determined along with the full deflector flow field. The general nature of this method provides the capability to capture all of the essential features of complex geometries found in typical fire sprinklers, at a fraction of the computational cost of a traditional CFD calculation. This reduction in computataional cost allows the quick exploration of the governing parameters for fire sprinkler head flow.

The hypothetical axisymmetric case explored in this study exemplifies the impact of geometric details of the sprinkler (and their associated boundary values) on the deflector flow. Specifically, the impact of slot area and slot centroid radius on the sprinkler head flow split was demonstrated in this study, as well as the impact of this geometry on fluid sheet thickness and trajectory. This flow split is critical as the sheet topology (i.e. location, thickness, and velocity), which governs initial spray details, is completely determined from this quantity. The model developed in this study is capable of capturing this fundamental sheet formation behavior

quantitatively with only minimal computational burden.

The potential to completely predict fire sprinkler sprays opens the door for large advancements. If sprinkler sprays can be predicted, than sprinklers can be designed rather than just tested. If sprinkler sprays can be predicted, than models can account for the impact of sprinkler spray performance. Predicting sprinkler performance is a large piece in the fire protection engineering puzzle and predicting the impingement of a jet on a sprinkler head is a large portion of prediciting sprinkler performance. The sprinkler head deflector flow model is an essential component of a high-fidelity modeling framework capable of completely describing the initial sprinkler spray.

Further work on this problem includes additional model development, the expansion to capture the periodic geometry (i.e. tines and slots) typical of real fire sprinklers, experimental validation, and incorporation into the complete sprinkler model as outlined in Fig. 1.1.

A large amount of future work is required to expand this model into a useful component of sprinkler design. To begin, large improvements in error could be expected with the incorporation of an adaptive free surface shape model. The present model for free surface shape is only a first order approximation. By adapting the free surface shape to reflect calculated conditions the total potential flow predictions could be dramatically improved. An adaptive shape for the free surface is also a necessary component to a three dimensional version of the sprinkler deflector model. A typical fire sprinkler head has a periodic geometry of slots and tines that is not well represented by the ring slot formulation explored above. An expansion to three

dimesions would improve the usefulness of the entire model.

Validation, in addition the the verifcation performed in section 3.2, would be useful for affirming the results of the presented model. Experimental measurement of a ring slot sprinkler could serve to lend further insight into the shape of the free surface, the deviation from potential flow, as well as measurements of flow splits for a number of slot configurations.

Lastly, the sprinkler deflector model is merely the first portion of a complete model. The flow splits and sheet characteristics determined by deflector models are an essential component to determining droplet size within the sheet breakup model and fragment distribution in the fragment transport model. With a complete model of sprinkler behavior, further insight into sprinkler design and sprinkler performance can be gained.

Bibliography

[1] N. Ren, a. Blum, Y. Zheng, C. Do, and a. Marshall. Quantifying the Initial Spray from Fire Sprinklers. *Fire Safety Science*, Vol. 9:pp. 503–514, 2008.

[2] N. Ren and A. W. Marshall. Characterizing the initial spray from large Weber number impinging jets. *International Journal of Multiphase Flow*, Vol. 58:pp. 205–213, 2014.

[3] G. K. Batchelor and A. E. Gill. Analysis of the stability of axisymmetric jets, 1962.

[4] F. Savart. *Ann. Chim. Phys.*, 1931.

[5] Lord Rayleigh. On the Capillary Phenomena of Jets. *Proceedings of the Royal Society of London*, Vol. 29:pp. 71–97, 1879.

[6] Weber. Zum zerfall eines flssigkeitsstrahles. *angew. Math Mech*, 1931.

[7] H. Squire. Investigation of the instability of a moving liquid film. 4, 1953.

[8] Shea J. F.. Hagerty, W. W. A Study of Stability of Plane Fluid Sheets. *Journal of Applied Physics*, Vol. 22:pp. 509–514, 1955.

[9] Hasson D. Ward D.E. Dombrowski, N. Some Aspect of Liquid Flow through Fan Spray Nozzles. *Chemical Engineering Science*, Vol. 12:pp. 35–50, 1959.

[10] Hooper P.C. Dombrowski, N. The Effect of Ambient Density on Drop Formation in Sprays. *Chemical Engineering Science*, Vol. 17:pp. 291–305, 1962.

[11] Hooper P.C. Dombrowski, N. The Aerodynamic Instability and Disintegration of Viscous Liquid Sheets. *Chemical Engineering Science*, Vol. 18:pp. 203–214, 1963.

[12] Tankin R.S. Li, X. On the Temporal Instability of a Two-Dimensional Viscous Liquid Sheet. *Journal of Fluid Mechanics*, Vol. 226:pp. 425–443, 1991.

[13] J. C. P. Huang. The break-up of axisymmetric liquid sheets. *Journal of Fluid Mechanics*.

[14] Villermaux E. Clanet, C. The life of a smooth liquid sheet. *Journal of Fluid Mechanics*, Vol. 462:pp. 307–340, 2002.

[15] Clanet C. Villermaux, E. Life of a flapping liquid sheet. *Journal of Fluid Mechanics*, Vol. 462:pp. 341–363, 2002.

[16] W. Schach. Umlenkung eines kriesfoermignen fluessigkeitsstrahes an einer eben platte senkrecht zur stroemunsrichtung. *Ing. Arch.*, Vol. 6:pp. 51–59, 1935.

[17] Fr. Reich. Deflection of a free liquid jet on a flat plate perpendicular to the floor direction. *VDI Research Journal.*, Vol. 290, 1926.

[18] Wendt B. Prahl, J. M. Discharge distribution performance for an axisymmetric model of a fire sprinkler head. *Fire Saftey Journal*, Vol. 14:pp. 101–111, 1988.

[19] Nichols B. D. Hirt, C. W. Volume of fluid (vof) method for the dynamics of free boundaries. *Journal of Computational Physics*, Vol. 39:pp. 201–225, 1979.

[20] N. T. Bloomer. Note on the position of ring singularities in an axisymmetric potential field. *Journal of Fluid Mechanics*, Vol. 3:217, 2006.

[21] H. Y. Chang and J. F. Conly. Potential flow of segmental jet deflectors. *Journal of Fluid Mechanics*, Vol. 46(03):pp. 465, 2006.

[22] K D Steckler, H R Baum, and J G Quintiere. Fire Induced Flows Through Room Openings - Flow Coefficients. *Twentieth Symposium on Combustion*, pages pp. 1591–1600, 1984.

[23] A. Elcrat and L. Zannetti. Models for inviscid wakes past a normal plate. *Journal of Fluid Mechanics*, Vol. 708:pp. 377–396, 2012.

[24] J. H Lienhard and J. H Lienhard. Velocity Coefficients For Free Jets From Sharp-Edged Orifices. *Journal of Fluids Engineering*, Vol. 106:pp. 13–17, 1984.

[25] T. L. Labus. Liquid jet impingement normal to a disk in zero gravity. *NASA Technical Paper.*, 1017, 1977.